

Clear-column closure studies of aerosols and water vapor aboard the NCAR C-130 in ACE-Asia, 2001

J. Redemann¹, S. Masonis², B. Schmid¹, T. Anderson², P. Russell³, J. Livingston⁴, O. Dubovik⁵, A. Clarke⁶

Corresponding author: Jens Redemann
Bay Area Environmental Research Institute
NASA Ames Research Center
MS 245-5
Moffett Field, CA 94035-1000
Phone: +1 805 658 2637
Fax: +1 805 658 2637
e-mail: jredemann@mail.arc.nasa.gov

Affiliations:

¹ Bay Area Environmental Research Institute, 560 3rd Street West, Sonoma, CA 95476. (e-mail: jredemann@mail.arc.nasa.gov, bschmid@mail.arc.nasa.gov)

² Department of Atmospheric Sciences, University of Washington, Box 351640, Seattle, WA 98195-1640. (e-mail: sarahd@atmos.washington.edu, tadand@atmos.washington.edu)

³ NASA Ames Research Center, MS 245-5, Moffett Field, CA 94035-1000. (e-mail: prussell@mail.arc.nasa.gov)

⁴ SRI International, 333 Ravenswood Avenue, Menlo Park, CA 94025. (e-mail: jlivingston@mail.arc.nasa.gov)

⁵ Goddard Earth Sciences & Technology Center, NASA Goddard Space Flight Center, Code 912, Greenbelt, MD 20771. (email: dubovik@aeronet.gsfc.nasa.gov)

⁶ Department of Oceanography, University of Hawaii, 1000 Pope Rd., Honolulu, HI 96822. (e-mail: tclarke@soest.hawaii.edu)

Abstract. Column closure studies are a tool to assess whether in situ and remote measurements of aerosol optical properties on a given aircraft are mutually consistent. In this paper we describe aerosol and water vapor column closure studies based on instrumentation flown aboard the NCAR C-130 aircraft in the ACE-Asia field experiment in March-May, 2001. For in situ observations, aerosol particles were sampled through a newly-designed low turbulence inlet (LTI). In 28 profiles extending to altitudes of up to 8km, the in situ observations of scattering and absorption were compared to measurements with the six-channel NASA Ames Airborne Tracking Sunphotometer, AATS-6. The comparison of sunphotometer and in situ derived layer aerosol optical depth (AOD) at 550 nm showed agreement (closure) within the measurement uncertainties in 25 out of 28 case studies. The average difference in layer AOD derived from the two methods was 0.03, corresponding to an average difference of 11.5%. The uncertainties in AATS-6 derived layer AOD ranged between 5 and 59% (with a mean of 22%), and for the first time included an estimate for the uncertainty in layer AOD caused by possible horizontal variability in AOD encountered in the vertical profile. The average uncertainty in AATS-6 derived layer AOD due to possible horizontal variability alone was 19%. The uncertainties in in situ derived layer AOD were between 10 and 55% (with a mean of 19%). Stratification of the extinction closure data by ambient relative humidity (RH) revealed that in situ derived aerosol extinction at low ambient relative humidity (<20%RH) tended to be slightly less than sunphotometer derived aerosol extinction, while in situ derived aerosol extinction at higher relative humidity was slightly greater than the sunphotometer derived values. Stratification of the extinction closure data by the fine mode fraction of scattering indicated a modest enhancement of coarse-mode extinction in the combined LTI/plumbing system. Analogous closure studies for layer water vapor and water vapor density showed that AATS-6 measured these quantities with very high accuracy, with correlation coefficients of 0.989 and 0.955 (rms differences of 10% and 33%), respectively.

1. Introduction

The Spring 2001 phase of the Asian Pacific Regional Aerosol Characterization Experiment (ACE-Asia), studied aerosol outflow from the Asian continent to the Pacific basin. It was designed to integrate suborbital and satellite measurements and models so as to reduce the uncertainty in calculations of the climate forcing due to aerosols [Huebert *et al.*, 2002]. ACE-Asia included various aircraft, ground-based and ship-based observations in close coordination with satellite overpasses. The close coordination of measurements on the various platforms was intended to yield important insights into the spatial and temporal variability of Asian aerosols as they are transported into the Pacific Basin troposphere. In particular, the vertical distribution of aerosols and hence the vertical distribution of their climatic impact needs to be determined in order to assess aerosol climate interactions [Hansen *et al.*, 1997, Ramanathan *et al.*, 2001].

To assess whether or not the instrumentation aboard the various participating aircraft measured an adequate representation of the ambient aerosol, extinction and optical depth closure studies need to be carried out. Previous closure studies have advanced our understanding of in situ aerosol measurement methods in field experiments, such as the Tropospheric Aerosol Radiative Forcing Observational Experiment, TARFOX [Hegg *et al.*, 1997; Hartley *et al.*, 2000], the 2nd Aerosol Characterization Experiment, ACE-2 [Collins *et al.*, 2000, Schmid *et al.*, 2000], the Indian Ocean Experiment, INDOEX [Masonis *et al.*, 2002] and the Southern African Regional Science Initiative, SAFARI 2000 [Magi *et al.*, 2002].

This paper describes closure studies based on instrumentation flown aboard the NCAR C-130 aircraft in research flights from March 30, 2001 to May 4, 2001. The aircraft was based at the Marine Corps Air Station, Iwakuni, Japan (34.144N, 132.236E). In particular, we report on the comparison of aerosol extinction determined by differentiation of vertical profiles of aerosol optical depth measured using the six-channel NASA Ames Airborne Tracking Sunphotometer,

AATS-6, to aerosol extinction measured in situ using a combination of nephelometers to determine aerosol scattering and Particle Soot Absorption Photometers (PSAP) to determine aerosol absorption. Vertical integration of the in situ derived aerosol extinction profiles yielded layer aerosol optical depth, which was compared directly to the sunphotometer AOD measurements.

The closure studies described here are a test of both the in situ and sun photometer measurement methods, as both measurement techniques have strengths and weaknesses. For example, in determining aerosol extinction from the AATS-6 measurements of aerosol optical depth, one needs to be concerned with the possible horizontal inhomogeneity in aerosol properties encountered along the vertical profile, since it may be misinterpreted as a vertical variation in aerosol properties. In addition, the required smoothing of AATS-6 aerosol optical depth profiles makes it impossible for this technique to capture very strong vertical gradients in the aerosol field. The in situ measurements on the other hand, are subject to losses or enhancements of particles in the combined inlet/plumbing system, through which the aerosols are sampled. Further, the aerosol is usually dried out in the in situ sampling process, necessitating the humidification of dry scattering measurements. The in situ aerosol sampling system aboard the NCAR C-130 aircraft used a newly-designed low-turbulence inlet (LTI) [Huebert et al., this issue], which was built to reduce inertial impaction losses of large aerosol particles in the inlet itself. Indeed, the closure studies carried out here represent a test of the performance of the aerosol sampling system in accounting for all particles responsible for ambient light extinction, as well as a check of the assumptions and corrections that both measurement methods are subject to. We would like to point out that most previous attempts at aerosol column closure studies were confined to a total of 10-12 vertical profiles. In this paper, however, we present a total of 28 profiles, which ultimately allowed the stratification of the data by ambient relative humidity (RH) and aerosol fine mode scattering fraction (defined here as the

fraction of dry light scattering due to aerosols smaller than 1 μ m in diameter). The amount of data available and hence the stratification by the above quantities permitted further insight into the performance of both measurement techniques.

2. Instrumentation and Methodology

2.1 Measurements of aerosol optical depth with the NASA Ames Airborne Tracking

Sunphotometer, AATS-6

2.1.1 Instrument description

In ACE-Asia, the 6-channel NASA Ames Airborne Tracking Sunphotometer (AATS-6) [Matsumoto *et al.*, 1987] operated on 15 of the 19 research flights of the NCAR C-130, while its 14-channel counterpart (AATS-14) flew successfully on 19 research flights of the CIRPAS Twin Otter [Schmid *et al.*, this issue]. AATS-6 measures direct solar beam transmission at 6 wavelengths (380.1, 450.9, 525.7, 864.5, 941.9, 1021.3 nm), yielding aerosol optical depth (AOD) spectra and column water vapor (CWV). For examples of data obtained with the two AATS instruments in recent field campaigns the interested reader is referred to Russell *et al.*, 1999, Schmid *et al.*, 2000, Livingston *et al.*, 2002, Schmid *et al.*, 2002, Redemann *et al.*, 2002. Details that pertain to the analysis of AATS-14 data obtained in ACE-Asia are described in Schmid *et al.* (this issue).

AATS-6 is designed to operate on a variety of aircraft. Once pointed to a position in the sky within 30 degrees of the sun, it can track the sun without input from an operator and record data in a self-contained data system. In addition, it must interface to an aircraft-provided data system, and receive and execute commands from a remote operator station (laptop), and transmit science and instrument-status data to that station. Using aircraft-provided data on latitude, longitude and ambient static pressure, aerosol (or particulate) optical depth $\tau_p(\lambda)$ and columnar water vapor CWV are computed in real-time and displayed at the operator station (along with

raw data, instrument status, and aircraft-provided data). In AATS-6, azimuth and elevation motors controlled by differential sun sensors rotate a tracking head so as to lock on to the solar beam and keep detectors normal to it. The tracking head of the instrument mounts external to the aircraft skin, to minimize blockage by aircraft structures and also to avoid data contamination by aircraft-window effects. Each channel consists of a baffled entrance path, interference filter, photodiode detector, and preamplifier, which are temperature-controlled to avoid thermally-induced calibration changes.

2.1.2 Data reduction

The most recent deployments of AATS-6 include the Tropospheric Aerosol Radiative Forcing Observational Experiment (TARFOX) in July 1996 [*Russell et al.*, 1999a,b] and the Puerto Rico Dust Experiment in September 2000 [*Livingston et al.*, 2002]. AATS data processing conceptually consists of two steps. First, the determination of a calibration that is consistent with pre- and post-mission calibration (as well as high altitude AOD spectra measured during the field deployment); and second, the actual data reduction which consists of (i) the application of a cloud-screening algorithm to the measurement signals, (ii) the separation of gaseous attenuation and aerosol contributions to the slant-path transmission measurements, and (iii) the correction of aerosol optical depth for diffuse light entering the sunphotometer field of view in addition to the direct solar beam. A general description of the methods for AATS data reduction and error analysis can be found in *Russell et al.*, 1993a, *Schmid and Wehrli*, 1995, and *Schmid et al.*, 2002. A brief summary is given here.

Radiometric calibration is generally determined from Langley plots [*Schmid and Wehrli*, 1995] at high-mountain observatories. Pre- and post-mission calibration for the ACE-Asia field campaign was determined via Langley plots using data taken at the high-altitude Mauna Loa Observatory (MLO) in March and June of 2001, respectively. For AATS-6, comparison of pre-

and post-mission calibration constants, inspection of high-altitude AOD spectra in addition to in-flight and ground-based comparisons to AATS-14 revealed that pre-mission calibration constants need to be used for flights until April 12, 2001 (NCAR C-130 flight RF07), from which point on post-mission calibration should be applied. Because of occasional poor tracking performance of AATS-6, a tracking uncertainty of 2% was added to the uncertainties in the calibration constants.

The AATS-6 channels are chosen to allow separation of aerosol and water vapor. From the slant-path transmissions we retrieve $\tau_p(\lambda)$ in 5 narrow (about 5 nm bandwidth) wavelength bands centered at 380.1, 450.9, 525.7, 864.5, and 1021.3 nm and the columnar amounts of water vapor. The 864nm channel, which was most affected by poor tracking performance of AATS-6, is excluded from consideration in this paper and is excluded from the ACE-Asia archive. In addition to the corrections for Rayleigh scattering and O₃ absorption, some channels require corrections for NO₂, H₂O and O₂-O₂ absorption. Cross-sections were computed using LBLRTM 6.01 [Clough, and Iacono, 1995] with the CKD 2.4.1 continuum model using the HITRAN 2000 (v 11.0) line-list [Rothman *et al.*, 2001] (including an update for water vapor from 04/2001, see <http://www.hitran.com/hitran/updates.html>). NO₂ cross-sections not included in LBLRTM 6.01 were taken from Harder *et al.* [1997]. NO₂ was assumed constant at 2×10^{-15} molecules cm⁻². Daily observations of total ozone column content were taken from the Total Ozone Mapping Spectrometer (TOMS) on the Earth Probe satellite, and ranged between 327 and 362 Dobson Units during the entire field campaign.

During ACE-Asia, AATS-6 data were recorded every 4 seconds consisting of an average and standard deviation of 9 samples taken during the first 3 of the 4 seconds. The standard deviations were used in our cloud-screening algorithm that is based on clouds exhibiting higher standard deviations than clear sky.

Because sunphotometers have a nonzero field of view (FOV), they measure some diffuse light in addition to the direct solar beam. As a result, uncorrected sunphotometer measurements

can overestimate direct-beam transmission and hence underestimate $\tau_p(\lambda)$. For most aerosol conditions and sunphotometer FOVs these effects are negligible. For example, *Eck et al.* [1999] report that for the AERONET sun/sky radiometers, which have FOV half-angle 0.6° , the diffuse-light correction to apparent $\tau_p(\lambda)$ is $<0.7\%$ of $\tau_p(\lambda)$, even for desert dust with effective (area-weighted) radius as large as $1.75 \mu\text{m}$. The Ames Airborne Tracking Sunphotometers, AATS-6 and -14, are designed and built with a relatively large FOV (measured half-angle 1.85°) to help keep the full solar disk in view when sun-tracking during aircraft maneuvers. This larger FOV makes it necessary to assess quantitatively the diffuse light effects on AATS-derived $\tau_p(\lambda)$ when large particles are dominant. We have previously done this for post-volcanic stratospheric aerosols [*Russell et al.*, 1993a,b] and for the Saharan dust encountered in the Puerto Rico Dust Experiment (PRIDE) [*Livingston et al.*, 2002].

To quantify the diffuse light effects for the aerosols prevalent during ACE-Asia we used the analytical formulation of *Shiobara and Asano* [1994] and *Kinne et al.* [1997] to calculate $\tau_p(\lambda)$ correction factors

$$C = \tau_p(\lambda) / \tau_p(\lambda)' \quad (1)$$

where $\tau_p(\lambda)'$ is apparent (uncorrected) $\tau_p(\lambda)$. Our calculations used the AATS-6 FOV (half-angle 1.85°) and aerosol scattering phase functions derived both from (1) size distributions and compositions measured on the Twin Otter in ACE-Asia [*Wang et al.*, 2002] and (2) size distributions and complex refractive indices retrieved from Sun and sky radiance measurements by AERONET stations [*Holben et al.*, 1998, *Dubovik et al.*, 2002] in the ACE-Asia region during Spring 2001.

We found that the correction factors were well correlated with Ångström exponent

$$\alpha(\lambda_1, \lambda_2) = -\ln[\tau_p(\lambda_1)/\tau_p(\lambda_2)]/\ln(\lambda_1/\lambda_2), \quad (2)$$

and that the correlation improved as wavelengths λ_1 and λ_2 increased. (Evidently this is because longer wavelengths are more sensitive to the larger particles in a distribution, and the larger particles are responsible for the diffuse light effects). Scatter plots of $C-1$ versus α were well fitted by exponentials of the form

$$f = C-1 = A \exp(-B\alpha). \quad (3)$$

Hence we corrected each individual $\tau_p(\lambda)'$ measurement using the wavelength dependent correction factor f with α (using $\lambda_1 = 380$ nm and $\lambda_2 = 1020$ nm) of the overlying aerosol column as input. The correction factor f decreases with increasing wavelength. For the shortest AATS-6 wavelength (380.1 nm), 90% of all τ_p' had to be corrected by less than 5.1%, with 40% of all τ_p' requiring less than 3% correction. To illustrate, a 5% correction to a τ_p' of 0.3 is 0.015. Uncertainties in the diffuse-light correction factors, based on the standard deviations of α -grouped values of C calculated from the AERONET and Twin-Otter data sets, were included in the overall uncertainty of $\tau_p(\lambda)$ using Eqn.(A22a) of *Russell et al.*[1993b].

Vertical differentiation of the AOD and CWV data in suitable flight patterns yields vertical profiles of aerosol extinction and water vapor concentration, respectively. The general procedure for deriving aerosol extinction profiles involves fitting the vertical AOD profiles with smoothed cubic spline functions, which are then differentiated with respect to altitude.

Figure 1 shows the location of 28 profiles flown by the NCAR C-130, which have been determined to be suitable for a comparison of the AATS-6 derived aerosol optical depth and extinction to in situ measured values of the same variables (the in situ derived layer aerosol optical depth is determined by vertical integration of the in situ measured extinction profiles, cf. next section). In determining the suitability of these profiles for a closure study, we observed the quality of in situ and sunphotometer data in these profiles and sought to minimize the

obscuration of AATS-6 by clouds. In fact, for all profiles that were considered suitable from the AATS-6 perspective, in situ data were readily available.

Figure 2 shows the vertical profiles of $\tau_p(\lambda)$ at four wavelengths (380.1, 450.9, 525.7, and 1021.3nm), while Figure 3 shows the derived vertical profiles of aerosol extinction, $\sigma_{ep}(\lambda)$, at the same wavelengths. To derive aerosol extinction at 550nm for an easy comparison to in situ derived aerosol extinction at 550nm, the aerosol optical depth spectra at each altitude were first fit with an Ångström law to derive a profile of $\tau_p(550\text{nm})$. In a second step, the profile of $\tau_p(550\text{nm})$ was fit with a smoothed cubic spline curve which was then differentiated to yield the vertical profile of $\sigma_{ep}(550\text{nm})$.

2.1.3 Uncertainty in sunphotometer retrievals

The total uncertainty of the retrieved $\tau_p(\lambda)$, due to uncertainties in calibration, tracking performance, signal measurement, airmass computation, diffuse light correction, and corrections of molecular scattering and absorption, was computed following the procedures given by *Russell et al.* [1993a]. The uncertainty in CWV was computed following *Schmid et al.* [1996].

The main sources of uncertainty in the AATS-6 derived extinction are due to (i) potential misinterpretation of cloud optical depth as aerosol optical depth, (ii) horizontal inhomogeneity along the measurements that comprise a vertical profile (i.e., when the location of two AOD measurements along the profile are horizontally separated) and (iii) the constraints of fitting smoothed curves through the profiles of aerosol optical depth. Out of these sources of uncertainty (i) is minimized by our general cloud screening technique, which filters consecutive AATS-6 $\tau_p(\lambda)$ measurements with standard deviations above a certain threshold level as clouds, assuming that clouds generally exhibit larger spatial variability. In cases of doubt, the Ångström exponent, which is close to zero for clouds, was considered. The uncertainty caused by (iii) will

affect the AATS-6 derived extinction only at altitudes where there is a strong vertical gradient in aerosol light extinction.

Of biggest concern, because not directly measurable, is the potential uncertainty in AATS-6 derived aerosol extinction due to horizontal inhomogeneity in the aerosol field during the vertical profile measurements. Because the AATS-6 extinctions are computed from the increase in aerosol optical depth with decreasing altitude, there is the possibility that an aerosol plume suddenly enters the sunphotometer-to-sun path at a higher altitude and the increase in $\tau_p(\lambda)$ is interpreted as aerosol extinction at the altitude of the airplane. However, depending on flight track, wind conditions and inhomogeneity in the aerosol field, such an aerosol plume must not have necessarily been measured by the in situ instrumentation on the same aircraft. To illustrate the effect of horizontal inhomogeneity on AATS-6 derived layer AOD, assume that the aircraft traverses a horizontal gradient, g , in aerosol optical depth while flying a vertical profile. If the aircraft carrying AATS traveled a horizontal distance, Δx , while making the profile measurements of τ_p , the uncertainty in layer AOD due to a horizontal aerosol gradient would be given by:

$$\delta_g \tau = \pm g \cdot \Delta x \cdot \bar{\tau} \quad (7)$$

where $\bar{\tau}$ is the mean AOD measured in the layer. For example, for an arbitrary gradient in AOD of 10% per 100km, a horizontal distance of 50 km traveled during a vertical profile and a mean AOD of 0.2 in a given layer, the gradient uncertainty computed using Eqn.(7) is 0.01. Incidentally, $g(525\text{nm})$ computed during low level legs on 11 flights ranged from 1 to 14% at 525 nm, with a mean of 6% per 100km. A publication on the topic of AOD variability in ACE-Asia is forthcoming.

In analogy to Eqn.(7), the uncertainty due to a horizontal gradient in AATS-6 derived extinction from two measurements of τ , separated by a small vertical distance Δz can be written as:

$$\delta_g \sigma_{ext} = \pm \frac{g \cdot \Delta x \cdot \tau_{top}}{\Delta z} \quad (8)$$

where τ_{top} , is the aerosol optical depth at the higher altitude of the two AOD measurements. The sign in Eqn.(7) and (8) depends on the orientation of the aerosol gradient denoted by g . Generally, the uncertainty in the difference of two measurements of $\tau_p(\lambda)$ at different altitudes, due to uncertainties in calibration, signal measurement, airmass computation, and corrections of molecular scattering and absorption would be negligible due to the fact that these uncertainties represent merely a bias in the measurements. However, AATS-6 frequently exhibited poor tracking performance and it cannot be assumed that uncertainties in tracking are equal at the top and the bottom of a profile. From observations of AOD irregularities in select channels, we concluded that in general, the tracking performance uncertainties were less than 0.02 at airmasses around 1. Because the dominating source of uncertainty, i.e., the calibration uncertainty, was of equal magnitude, we decided to use the root-square-sum of half of the total AOD uncertainties (instrumental plus tracking), $\delta\tau$, at the top and the bottom of a given profile as an additional term in the uncertainty in layer AOD, viz.:

$$\delta_r \tau = \sqrt{\left(\delta\tau(z_1)/2\right)^2 + \left(\delta\tau(z_2)/2\right)^2} \quad (9)$$

Finally, the total error in layer AOD from AATS-6 is the root-square-sum of the two terms given in Eqn.(7) and (9).

2.2 In situ measurements of aerosol scattering and absorption

2.2.1 Instrument description

Aboard the NCAR C-130, a suite of instruments was used to carry out in situ measurements of aerosol light scattering and absorption. Two integrating nephelometers (TSI Inc., Model 3563) measured integrated total scatter at 450, 550, and 700nm wavelengths

(Anderson *et al.*, 1996; Anderson and Ogren, 1998). One nephelometer always measured all aerosol, while the second nephelometer usually measured only aerosol of dry aerodynamic diameter $D < 1\mu\text{m}$. Two Radiance Research, Inc. Particle Soot Absorption Photometers were used to measure light absorption by aerosols at 550nm (Bond *et al.*, 1999). For the C-130 research flights 6-19, one PSAP measured the total aerosol and the other measured only aerosol of dry aerodynamic diameter $D < 1\mu\text{m}$. All of the measurements described so far were made at low (nearly always $< 45\%$) relative humidity and are described in more detail by Anderson *et al.* [this issue]. A separate measurement of the increase in 540nm integrated light scattering with relative humidity was made using two model M903 Radiance Research nephelometers. One of the Radiance nephelometers was run at low ($< 45\%$) RH and the other at $85\% \pm 2\%$ RH. By assuming an exponential fit (see below) to the increase in light scattering with RH (Kasten, 1969), $f(\text{RH})$, we were able to use this two-point data to determine $f(\text{RH})$ and thus predict light scattering at ambient relative humidity. This is important in the context of this closure study because the sun photometer measures light extinction by aerosols under ambient conditions.

2.2.2 In situ data reduction

Light scattering at 550nm and ambient RH was calculated from the dry TSI nephelometer-derived scattering at 550nm using the following formulation:

$$\sigma_{sp}(550\text{nm}, \text{RH}_{amb}) = \sigma_{sp}(550\text{nm}, \text{RH}_{dry}) \cdot f_{RH} \quad , \quad (4)$$

where

$$f_{RH} = \left(\frac{100 - \text{RH}_{amb}}{100 - \text{RH}_{dry}} \right)^\gamma \quad (5)$$

The parameter γ in equation (5) is derived using scattering values from the Radiance Research nephelometers as:

$$\gamma = \frac{\ln[\sigma_{spr}(540nm, wet) / \sigma_{spr}(540nm, dry)]}{\ln[(100 - RH_{dry}) / (100 - RH_{wet})]} \quad (6)$$

Because the effect of humidification on light absorption was not measured, light absorption data are not adjusted to ambient RH. In addition, the only currently available modeling studies by *Redemann et al.* [2001] suggest that absorption humidification factors for a range of atmospheric conditions are likely negligible (i.e., at most favorable conditions, absorption humidification factors for an increase in RH from 30 to 80% were between 7 and 15%).

The data reported here have been averaged to 10-second resolution. In order to improve the signal-to-noise ratio, the light absorption data have additionally been smoothed over a 30-sec shifting window. Similarly, the humidified scattering measurements by the Radiance Research nephelometers are filtered through a smoothing function with an approximately 20-second response time. Data from the TSI integrating nephelometers were processed using eight span gas (air and CO₂) calibrations to determine corrections to the gain and offset calibration coefficients. Calibration corrections were applied on a flight-by-flight basis. Angular truncation correction factors were applied as recommended by *Anderson and Ogren* (1998). Data from the Radiance Research nephelometers were also adjusted for calibration changes using span gas measurements. Additionally, in-flight filtered air measurements were used to adjust the Radiance nephelometers' calibration on the first two flights to account for changes in calibration that occurred between span gas calibrations. Note that the angular sensitivity function for the Radiance Research nephelometers has not yet been carefully quantified and issues in understanding the absolute value of the Radiance nephelometer scattering measurement for the coarse mode remain unresolved. Hence, angular correction factors have not been applied to these data. However, based on a preliminary assessment of the Radiance nephelometers' angular truncation range done in the UW lab and measurements of the RH dependence of the Ångström

exponent during ACE-Asia (*Carrico et al.*, this issue), we feel confident that errors in the derived values of γ , and hence $f(RH)$, should be small because there should not be a significant difference in the angular truncation corrections between the wet and the dry nephelometer measurements. For sub-micron aerosol, this is because the angular truncation correction factor is always small ($\sim 5\text{-}10\%$ of σ_{sp} maximum). Observations of the change in Ångström with RH for the ACE-Asia sub-micron aerosol indicate that there should be at most a 3% difference between the angular correction factors at 40% and 85% RH (*Carrico et al.*, this issue, Figure 6; *Anderson and Ogren*, 1998). For coarse mode aerosol, the fraction of light scattered into the near-forward direction does not change much with aerosol size so neither does the angular truncation correction factor. Additionally, the coarse mode aerosol measured from the C-130 during ACE-Asia was dominated by dust, which was not very hygroscopic ($f(RH) \sim 1.1$; *Anderson et al.*, this issue) so its size did not change much with RH.

Data from the Radiance Research Particle Soot Absorption Photometers (PSAPs) were corrected for spot size, flow rate, artifact response to scattering, and error in the manufacturer's calibration, all given by *Bond et al.* (1999). Light absorption, reported at standard temperature and pressure, were adjusted to ambient air density.

The sum of total aerosol 550nm-scattering adjusted to ambient RH, and aerosol 550nm-absorption yields ambient aerosol extinction at 550nm. Integration of vertical profiles of aerosol extinction with respect to altitude yields the layer aerosol optical depth at 550nm. This in situ derived layer aerosol optical depth can then be compared to the AATS-6 derived layer aerosol optical depth to determine the degree of closure between the in situ and sunphotometer measurements. In an additional closure test we compare the AATS-6 derived aerosol extinction at 550nm to the in situ derived extinction. We make both comparisons because extinction is more directly measured by the in-situ instruments, while optical depth is more directly measured by the sun photometer. Also presented herein are values of the Ångström exponent derived from

the TSI nephelometer data using an equation analogous to Eqn. 2, where τ_p is replaced by σ_{sp} as measured at low RH.

2.2.3 Uncertainty in in-situ data

The uncertainties in the in situ derived ambient extinction are due to instrumental uncertainties, uncertainties in the determination of $f(RH)$, and due to the uncertainty in losses of particles in the LTI (low turbulence inlet) or plumbing system through which the aerosols are sampled. For this study, the instrumental uncertainties are taken from *Anderson et al.* [this issue] and are described briefly below. We made no attempt to include the uncertainty due to the potentially imperfect transmission efficiency of the combined plumbing and inlet system. Initial laboratory measurements of the plumbing efficiency and theoretical calculations of the LTI performance suggest that the enhancement of large particles in the LTI system are largely compensated for by plumbing losses (*Anderson et al.*, this issue), such that only a $\sim 10\%$ enhancement in scattering is expected when coarse mode aerosol dominate scattering. Indeed, the closure studies carried out here are a partial test for the validity of such an assumption.

The 95% confidence interval uncertainty in the mean values were calculated for the scattering and absorption parameters, except for those derived from the Radiance Research nephelometers. Because the sources of measurement uncertainty for the Radiance Research nephelometers have not been quantified, we have fixed the uncertainty in γ at 0.2 and we calculate the uncertainty in $f(RH)$ and ambient-RH light scattering accordingly. Calculation of total uncertainty from multiple sources was made using standard propagation of errors under the assumptions that (i) each source of error is independent of the others such that they can be added in a sum-square sense and (ii) noise uncertainty decreases with the square-root of averaging time while all other sources of uncertainty do not change with averaging time. For the TSI integrating nephelometers, the following sources of uncertainty were considered: (i) instrument accuracy

[Anderson *et al.*, 1996], (ii) instrument calibration uncertainty [Anderson and Ogren, 1998], (iii) uncertainty in the angular truncation correction factors [Anderson and Ogren, 1998], (iv) uncertainty due to instrumental noise [Anderson and Ogren, 1998], (v) for total scattering at ambient RH, uncertainty in the adjustment from low to ambient RH, calculated using the assigned uncertainty in γ of 0.2. For the Particle Soot Absorption Photometers, the sources of uncertainty included were (i) instrument accuracy, (ii) instrument precision, (iii) uncertainty due to instrumental noise, and (iv) uncertainty in the applied scattering correction [Bond *et al.*, 1999].

2.3 Measurements of columnar water vapor with the NASA Ames Airborne Tracking Sunphotometer, AATS-6, and derivation of water vapor density

From the slant-path transmission in the AATS-6 wavelength band centered at 941.9nm we retrieve the amount of columnar water vapor, after the contributions of ozone absorption, Rayleigh scattering and aerosol attenuation have been removed. Cross-sections were computed using LBLRTM 6.01 [Clough, and Iacono, 1995] with the CKD 2.4.1 continuum model using the HITRAN 2000 (v 11.0) line-list [Rothman *et al.*, 2001] (including an update for water vapor from 04/2001, see <http://www.hitran.com/hitran/updates.html>). Differentiation of CWV data obtained in vertical profiles allows derivation of water vapor density ρ_w as a function of altitude.

2.4 In situ measurements of ambient absolute humidity

There were a number of redundant measurements of water vapor density aboard the NCAR C-130 in ACE-Asia. Humidity measurements were made using two collocated thermoelectric dew point sensors, two Lyman-alpha fast-response hygrometers and an experimental TDL laser hygrometer. As is typically the case, the two dew point sensors were set up differently to provide the best coverage under the widest range of ambient conditions. The first dew point sensor was set up for fast response, but its dynamic range was limited. The

second dew point sensor had a slower response but had the capability of measuring greater dew point depressions. A comparison of the data sets from these two sensors yielded generally good correlation in instrument signatures. However, some problems with water ingestion occurred which resulted in sensor drift. Each flight was evaluated on a case-by-case basis to see which dew point sensor was functioning the best on that particular flight. The selection of a reference humidity sensor for use in calculating all of the derived measurements was varied accordingly. When neither of the dew point sensors was considered to be working properly, the reference ambient humidity archived by the NCAR Research Aviation Facility (RAF) was derived from one of the two Lyman-alpha fast-response hygrometers. Effectively, the RAF reference humidity used in this paper was derived from a dew point sensor in flights RF01-03, 07, 09, 12, 14, 15, and 17-19, while the RAF reference humidity in flights RF04-06, 08, 10, 11, 13 and 16 was measured by one of the Lyman-alpha hygrometers. In analogy to the integration of in situ derived aerosol extinction profiles to yield layer aerosol optical depth, the in situ measured water vapor density can be integrated to yield layer water vapor, facilitating the comparison to AATS-6 derived layer water vapor.

3. Results

3.1 Comparison of aerosol extinction and layer aerosol optical depth at 550nm

Examining the AATS-6 derived aerosol extinction profiles in Figure 3, there are two types of profiles distinguishable. First, there are profiles which have a considerable amount of τ_p above an altitude of 2 km, usually caused by large dust particles (e.g., Figure3, panels j-t). Secondly, there are profiles, in which the total column aerosol optical depth is dominated by a strong contribution by mostly small particles in the boundary layer (e.g., Figure 3, panels a-h). The vertical stratification of these two aerosol types is more clearly seen in profiles of the Ångström law exponent, α , shown in Figure 4. The sun photometer-derived values, α_{ext} , are

fitted at each altitude to the AATS-6 derived extinction spectrum (blue dots in Fig. 4) where the in-situ values, α_{scat} , are derived using the low-RH scattering values at 450nm and 700nm (green dots in Fig. 4; See below for a discussion and quantitative comparison).

Figure 5 shows the comparison of AATS-6 derived profiles of aerosol extinction at 550 nm (blue lines and markers) to the in situ derived aerosol extinction at the same wavelength (green lines and markers). As described in section 2, the AATS-6 derived extinction was determined by first fitting an Ångström law to $\tau_p(\lambda, z)$ at each altitude, computing a profile of $\tau_p(550\text{nm}, z)$, cubic spline fitting this profile and finally differentiating the resulting smoothed spline fit. The in situ derived extinction is determined by humidifying the total dry scattering measurements at 550nm using Eqn.(4-6), then adding the PSAP absorption measurements at 550 nm.

The large suite of profiles shown in Figure 5 allows us to look for both systematic and intermittent sources of error in the measurements. The largest potential error sources for the in-situ measurements (i.e. inlet/plumbing efficiencies not equal to one and over- or under-humidification of light scattering from dry to ambient RH) are more likely to lead to systematic biases, whereas the largest potential sources of error in the AATS-6 measurements (i.e. the inability to capture strong vertical gradients and the misinterpretation of horizontal gradients in the aerosol field as vertical gradients) are more likely to lead to errors that are only present some of the time and will not always be in one direction. The latter type of error is demonstrated in Figure 5t, where the in situ instrumentation exhibits large vertical variation. It can be seen that the AATS-6 derived extinction cannot follow such a complex vertical profile. However, neglecting all other effects, the AATS-6 derived extinction should, over a broader vertical average, yield the true ambient value as illustrated by the fact that in Figure 5t the in situ derived extinction profile merely oscillates around the AATS-6 derived extinction profile. Similarly, in Figure 5e the sun photometer-derived extinction oscillates about zero in the 4-5km altitude

range; this could be due to a horizontal gradient in the aerosol viewed overhead as the aircraft ascended. Such intermittent errors are clearly seen in direct comparison profiles as given in Figure 5, but systematic biases and their potential sources will best be revealed by correlations between the two data sets.

In order to facilitate such a quantitative comparison, we first interpolated the AATS-6 extinctions to the altitudes at which the in situ measurements were reported. The 28 profiles shown in Figure 5 yielded a total of 3555 extinction data pairs. In a least square regression, we then sought to compare the two sets of data. The availability of ambient RH data, as well as the measurement of the fine mode scattering fraction allowed stratification of the extinction measurement comparisons by these quantities. Figure 6 shows the comparison of the two sets of extinction data stratified by ambient RH. The data were stratified in increments of 20% RH. Because neither method is error-free, we chose to apply not just a simple X-on-Y regression (model I), but we rather report the “least squares bisector”-line, calculated as the bisector of the minor angle between the two model I regressions: Y-on-X and X-on-Y, respectively [e.g., *Sprent and Dolby*, 1980]. The results of the model II regression analysis are given in Table 1. It can be seen that the extinction comparison for all RH (black solid line) is very close to the 1:1 line (black dashed line). The extinction comparison for ambient relative humidity between 0 and 20% seemed to exhibit larger extinction values determined by AATS-6 than by the in situ method, while the in situ method indicated more extinction than derived by AATS-6 for RH between 40 and 60% and for RH between 80 and 100%. However, since about 55% of the data were taken at RH below 20%, the overall agreement between the two methods is reasonable. It is noteworthy however, that the data below 20% RH exhibited the weakest correlation as indicated by the low r-square value of 0.467. In part, this scatter is caused by profile Figure 5s, which was apparently affected by large horizontal inhomogeneity. Leaving out the profile shown in Figure 5s resulted in a least square bisector fit-line with a slope of .87 and increased the r-square value to about .65

(not shown here). Hence, the general finding of lower in situ extinctions than AATS-6 derived extinctions would still hold true for RH between 0 and 20%.

Figure 7 shows stratification of the extinction comparison by the fine mode fraction of scattering, FFscat (here defined as the fraction of dry scattering due to aerosols smaller than 1 μm in diameter). Here we follow the stratification proposed by *Anderson et al.* [this issue], namely to divide the extinction data into three classes with FFscat below 30% (“coarse-dominated”), FFscat between 30 and 60% (“mixed”) and FFscat between 60 and 100% (“fine-dominated”). *Anderson et al.* [this issue] found that such a FFscat classification scheme tended to minimize the variability of most aerosol intensive properties. The total number of data points is less than that shown in Figure 6, because at very low aerosol concentrations, FFscat cannot be determined accurately. The r-square values of the extinction comparisons shown in Figure 7 indicate that the correlation between in situ and AATS-6 derived extinction improves as FFscat increases. The regression of fine-mode dominated extinctions (FFscat between 60 and 100%) is not just the best correlated of the three classes, it also shows a regression line with minimal offset (-0.004) and a slope closest to 1. This result suggests that it is most probable for the in situ instrumentation to measure an ambient extinction that is close to the sunphotometer derived values when the ambient aerosol is fine-mode dominated, and the result further indicates that there may be a bias towards over-sampling of large particles by the low turbulence inlet.

Integration of the in situ derived profiles of ambient aerosol extinction at 550 nm over vertical layers yields layer aerosol optical depth, $\tau_{l, is}$, at that wavelength. The differencing of two AATS-6 derived aerosol optical depths at the bottom and at the top of the same profiles yields AATS-6 derived layer aerosol optical depth, $\tau_{l, sp}$. Figure 8 shows the comparison of $\tau_{l, is}$ and $\tau_{l, sp}$ for the 28 profiles that comprise this closure study. The average difference in layer AOD derived from the two methods was 0.03, corresponding to an average difference of 11.5%. Due to the potentially more systematic nature of the uncertainties in the in situ derived extinctions, the

uncertainties in $\tau_{l, is}$ shown in Figure 8 were calculated as the vertical integral of the extinction errors. The uncertainties were between 10 and 55% (with a mean of 19%).

The error bars in AATS-6 derived layer optical depths are calculated using the root-square-sums of the instrumental uncertainty [cf. Eqn.(7)] and the “potential” gradient uncertainty [cf. Eqn.(9)]. “Potential” in this context is supposed to denote that we did not have independent measurements on horizontal AOD variability during these flight profiles and that the uncertainty in AATS-derived layer AOD was estimated using the horizontal variability measured during low-level flight legs in close temporal and spatial proximity to the actual profiles. Hence, the estimated uncertainties only exist if the exact variability seen during the low-level legs was also present during the vertical profiles. For illustration, the separate uncertainties from the instrumental and the gradient term are shown in Figure 8 as light and dark blue error bars, respectively. It is apparent that in the cases with large total uncertainties in $\tau_{l, sp}$, the uncertainty is dominated by the gradient uncertainty (dark blue). It turns out that this gradient uncertainty is not caused by large variability measured during the low-level flight leg to determine g in Eqn.(7), but due to the large horizontal distance Δx traveled during the vertical profile. The total uncertainties in AATS-6 derived layer AOD ranged between 5 and 59% (with a mean of 22%). The average uncertainty in AATS-6 derived layer AOD due to possible horizontal variability alone was 19%.

The model II least square bisector regression line for the layer aerosol optical depth comparison yields a fit line of $y = 0.94(\pm 0.098) + 0.005(\pm 0.026)$, with an r-square of 0.741 (solid blue line). Also shown for orientation are the 1:1 line (black dashed line) and model I (X-on-Y) regression result for a line without offset (blue dashed line). It is noteworthy that the model I, no-offset model yields a fit very similar to the least bisector result given above. We conclude that within the fit uncertainties, the layer aerosol optical depth comparison yields the same regression as the extinction comparison for all data points considered in Figure 7 (black

line) and note that neither the layer AOD nor the extinction regression produces a significant offset in the fit models.

3.3 Comparison of sunphotometer and in situ derived Ångström exponents

AATS-6 derived Ångström exponents were determined from least-square fits of the Ångström law to the four-wavelength aerosol extinction spectrum at each altitude as presented in Figure 3. At the same altitudes, the three-wavelength TSI nephelometer measurements of dry aerosol light scattering were fitted with the Ångström law to derive an in situ dry scattering Ångström exponent. Figure 9 shows the comparison of the two sets of data thus derived. Because both methods have considerable difficulty in determining Ångström exponents at very low aerosol loadings, we restricted the comparison to those altitudes where total aerosol extinction at 550nm was above 0.01 km^{-1} ($=10 \text{ Mm}^{-1}$), effectively reducing the total number of data points shown in Table 1 from 3555 to 2490. It can be seen in Figure 9 that there is considerable scatter in the Ångström exponent comparison ($r^2=0.62$). We attribute this fact to the fundamentally different techniques used to determine the two sets of Ångström exponents. The fit-model however, indicates line-fit parameters as shown in Table 3. It is evident that there is an offset of ~ 0.1 but a slope of nearly 1 to the model fit for all data points. Stratification of the data by low RH ($<40\%$, green lines) and high RH ($>40\%$, blue line) reveals the intuitive results that the offset is largely driven by data points with high RH. This result is intuitive, because the in-situ values of the Ångström exponent are derived from low-RH scattering and the humidification of the dry scattering would generally tend to produce smaller values of α_{scat} (i.e., larger, more humidified particles yield smaller Ångström exponents). Also, in general (i.e., for dry scattering Ångström exponents greater than zero), the addition of wavelength-independent aerosol absorption (an assumption just for illustration) to the three-wavelength scattering measurements would tend to produce extinction spectra that would yield smaller Ångström exponents. However, the addition of wavelength-dependent absorption may not produce any change in the Ångström exponent at

all. The fact that the offset is in the direction that can be expected when comparing dry-scattering derived Ångström exponents to ambient AATS-6 derived values, in conjunction with the fact that there is no considerable slope in the regression of the two data sets indicates again that there is no obvious size-dependent sampling bias in the in situ-derived representation of aerosol scattering properties.

3.4 Comparison of layer water vapor and absolute humidity

Columnar water vapor data from the AATS-6 941 nm channel transmission measurements was collected for the same 28 profiles as for the AOD measurements shown in Figure 2. Vertical differentiation yielded water vapor density, which was compared directly to the reference humidity measurements archived by the NCAR RAF (Research Aviation Facility). Figure 10 shows the comparison of vertical profiles of water vapor density from the sunphotometer (blue lines) to the in situ measurements (green lines). Because AATS measurements of columnar water vapor are possible through thin, homogeneous clouds, the number of CWV data points along a profile is generally higher than the number of AOD measurements along the same profiles. This fact explains the generally more structured appearance of the AATS-6 water vapor density profiles in Figure 10 by comparison to the AATS-6 extinction profiles in Figures 3 and 5.

It can be seen that both methods indicate water vapor density above 12 gm^{-3} for only two profiles (u and v), taken within 2 hours of each other on the same flight (RF16, April 30, 2001). All other profiles indicate relatively dry conditions with water vapor density below 12 gm^{-3} , in agreement with the low humidity measurements taken aboard the CIRPAS Twin-Otter aircraft [Schmid *et al.*, this issue].

Figure 11 shows the scatter plot comparisons between in situ derived layer water vapor and AATS-6 derived layer water vapor, while Figure 12 shows the same for the water vapor density along the profiles shown in Figure 10. We chose the in situ measurements as the

independent variable for both plots, because we ascertain that in situ observations of humidity are a much more direct measurement and hence the standard against which the remote method is to be tested. For the same reason, we chose to use a standard model I least-square linear regression of X-on-Y (which minimizes the squares of the distances in the y-direction only) of the form $y=mx+b$ (black solid lines in Figure 11 and 12). For comparison, Figures 11 and 12 also show the fit lines for linear models without offset (blue lines).

The regression of layer water vapor for the 28 profiles (cf. Figure 11) indicates a regression line of $y=0.95(\pm 0.020)+0.087(\pm 0.028)$, with a very high correlation coefficient r -square of 0.989. Both the fit parameters as well as the correlation coefficient are heavily influenced by the two high data points, which indicate slightly greater in situ derived layer water vapor measurements than the AATS-6 derived values. The comparison of water vapor density (6334 data points) shows a fit line with $y=1.02(\pm 0.003)+0.018(\pm 0.010)$, with a slightly smaller correlation coefficient of 0.955. The agreement found here is well below the precision limit of measuring water vapor using solar transmittance measurements in the 940 nm region [*Schmid et al.*, 1996] and hence must be considered, at least in part, to be fortuitous.

4. Summary and Conclusions

In this paper, we present 28 vertical profiles of aerosol optical depth and extinction at four wavelengths (380.1, 450.9, 525.7, 1021.3 nm), as well as profiles of columnar water vapor (CWV) and water vapor density measured by the NASA Ames Airborne Tracking Sunphotometer, AATS-6, aboard the NCAR C-130 in ACE-Asia.

In an aerosol column closure study, AATS-6 data collected in these 28 profiles were compared to aerosol extinction derived in situ from a combination of nephelometer aerosol scattering and PSAP aerosol absorption measurements. In analogy, the AATS-6 water vapor measurements were compared to the in situ humidity sensors aboard the same aircraft. A

companion paper describing the same efforts for data collected aboard the CIRPAS Twin-Otter aircraft is presented by *Schmid et al.* [this issue].

The AATS-6 measurements in ACE-Asia indicated generally dry conditions with the majority (26) of the profile studies indicating layer water vapor contents of less than 2 gcm^{-2} . The aerosol measurements showed two situations. First, a vertical distribution with pollution-dominated aerosols confined to the lower two kilometers and secondly, the scenario in which mineral dust particles produced significant mid-visible aerosol extinction at altitudes between 4 and 8 km. The notable advantage of the present study is the fact that the NCAR C-130 was able to penetrate into and frequently traverse the high-altitude mineral dust aerosol layers, enabling extinction comparisons within the dust.

The main goals of the aerosol column closure study were to check the mutual consistency between the sunphotometer and the in situ derived ambient aerosol extinction and layer optical depth. It should be noted that both methods bear significant advantages over the other and that the combination of the two data sets will likely further our understanding of Asian aerosol beyond the capabilities of either method on its own. Among the advantages of the in situ method of determining aerosol extinction (layer optical depth) are a generally better vertical resolution, better sensitivity at low concentration, and a frequently more robust measure of the wavelength dependence than AATS-6 was able to achieve in ACE-Asia. It should be noted that the latter two effects would have been less notable with an improved tracking performance of AATS-6 or the deployment of the newer AATS-14. Among the notable advantages of AATS-6 in determining ambient aerosol extinction is the fact that the aerosol does not need to be taken into the aircraft. Hence, there are no alterations of the ambient aerosol similar to the potential losses of particles in the in situ inlet/plumbing system, which required substantial theoretical corrections in previous closure studies. Hence, an aerosol column closure study is among other things a test of

the potential deficiencies of the two techniques involved. For the NCAR C-130 in ACE-Asia it was also a test of the newly-designed low turbulence inlet (LTI) system.

The comparison of in situ and sunphotometer derived layer aerosol optical depths at 550 nm yielded agreement within the measurement uncertainties (closure) for 25 of the 28 profiles. The uncertainties in AATS-6 derived layer AOD ranged from 5 to 59% (with a mean of 22%). It should be noted that the AATS-6 uncertainties due to the gradient uncertainties alone averaged ~19%. The uncertainties in in situ derived layer AOD were between 10 and 55% (with a mean of 19%). We attribute the lack of closure in the remaining three cases in part to spatial inhomogeneity beyond the level captured by the gradient uncertainty expression.

Comparison of the corresponding aerosol extinction values showed equally good agreement across the suite of profiles. Stratification of the extinction data by ambient RH revealed that the in situ derived aerosol extinctions were generally less than the AATS-6 derived values for RH between 0 and 20%, an RH range which accounted for about 55% of all data samples. The in situ derived extinctions generally exceeded the sunphotometer derived values in the RH ranges of 40 to 60% and 80 to 100%. These comparisons may indicate that the humidification corrections applied to the dry scattering measurements at low RH could be slightly low, but – even with this large suite of 28 profiles -- the regression is not statistically robust enough to state this with high confidence.

Stratification of the extinction comparison by the fine mode fraction of dry scattering, FF_{scat}, showed that the best agreement between the two methods, both in terms of correlation coefficient and in terms of the fit line being closest to the 1:1 line, was achieved for the fine-mode dominated cases and that the in situ values were somewhat higher in coarse-mode dominated cases. This result supports the general conception that aerosol closure studies are most successfully performed when dealing with small, spherical particles which pose the least challenges for either measurement technique [Magi *et al.*, 2002]. While again the statistics are

not robust enough to conclude definitively that there is a bias in the measurements, these results do indicate that the low turbulence inlet may have lead to an over-sampling of the coarse mode aerosol extinction by the in-situ instruments that is consistent with theoretical calculations (i.e. ~10%).

A comparison of Ångström exponents calculated from AATS-6 extinction spectra and nephelometer derived spectra of dry light scattering show generally good agreement, with an offset that can be explained by the fact that dry, in situ scattering spectra were used. The lack of a slope notably different from 1 in the general comparison of Ångström exponents thus derived also indicates that the two measurements techniques generally agreed on the size of particles responsible for the optical measurements. Hence, we conclude that AATS-6 and in situ observations of aerosol extinction aboard the NCAR C-130 are mutually consistent and that, on average, the in situ observation system, including its sampling component, can account for essentially all ambient aerosol extinction measured by AATS-6.

From the better agreement and tighter correlation in the comparison between AATS-6 derived water vapor to the in situ derived humidity measurements, we conclude that spatial inhomogeneity can only account for a small fraction of the scatter in the aerosol extinction and optical depth comparisons though. This conclusion assumes that the spatial variability in aerosol extinction and water vapor density are comparable. For future field experiments that are focused on column closure studies, we recommend the use of an inlet system equally capable of capturing aerosol extinction due to large particles as the LTI flown aboard the NCAR C-130 in ACE-Asia. We further suggest that flight patterns for closure studies either minimize the horizontal distance traveled during a vertical profile or include a low level horizontal leg in close succession with the vertical profile, to accommodate the assessment of the horizontal variability in aerosol optical properties.

5. Acknowledgments

We would like to thank S. Howell and C. McNaughton (both Univ. of Hawaii) for their help in the acquisition of scattering humidification data. We are indebted to S. Ramirez (BAERI, Sonoma, CA) for help in preparing some of the figures in this manuscript. We would like to thank Edward T. Peltzer (Monterey Bay Aquarium Research Institute, CA) for making available MATLAB shell-scripts for linear regression analysis (www.mbaeri.org/~etp3/regressindex.htm), and the National Center for Atmospheric Research, Research Aviation Facility (NCAR-RAF) for their support in the field on the C-130 aircraft and for providing their water vapor data for this analysis. We gratefully acknowledge funding provided to the NASA Ames sunphotometer group by NASA's Earth Observing System Inter-Disciplinary Science (EOS-IDS) Program, by the NASA's Radiation Sciences Program, and by the Office of Naval Research. Funding to the UW-Department of Atmospheric Sciences was provided by the National Science Foundation (grants ATM-0002198 and ATM-0138250) and by the National Oceanic and Atmospheric Administration (JISAO agreement NA37RJ0198).

6. References

- Anderson, T.L., D.S. Covert, S.F. Marshall, M. L. Laucks, R.J. Charlson, A.P. Waggoner, J.A. Ogren, R. Caldow, R. Holm, F. Quant, G. Sem, A. Wiedensohler, N.A. Ahlquist, and T.S. Bates, "Performance characteristics of a high-sensitivity, three-wavelength, total scatter/backscatter nephelometer", *J. Atmos. Oceanic Technol.*, 13, 967-986, 1996.
- Anderson, T.L., and J.A. Ogren, "Determining aerosol radiative properties using the TSI 3563 integrating nephelometer", *Aerosol Sci. Technol.*, 29, 57-69, 1998.
- Anderson, T.L., S.J. Masonis, D.S. Covert, N.C. Ahlquist, S.G. Howell, A.D. Clarke, and C.S. McNaughton, Variability of aerosol optical properties derived from in situ aircraft measurements during ACE-Asia, this issue.

- Bevington, P.R., and D.K. Robinson, Data Reduction and Error Analysis for the Physical Sciences, 2nd ed., McGraw-Hill, 1992.
- Bond, T.C., T.L. Anderson, and D. Campbell, "Calibration and intercomparison of filter-based measurements of visible light absorption by aerosols", *Aerosol Sci. and Tech.*, 30, 582-600, 1999.
- Carrico, C.M., P. Kus, M.J. Rood, P.K. Quinn, and T.S. Bates, Mixtures of pollution, dust, seasalt and volcanic aerosol during ACE-Asia: Light scattering properties as a function of relative humidity, submitted to JGR for publication in ACE-Asia Special Issue, 2003.
- Clough S. A., and M. J. Iacono, "Line-by-line calculations of atmospheric fluxes and cooling rates II: Application to carbon dioxide, ozone, methane, nitrous oxide, and the halocarbons," *J. Geophys. Res.*, 100, 16,519-16,535, 1995.
- Collins, D. R., Jonsson, H. H., Seinfeld, J. H., Flagan, R. C., Gassó, S., Hegg, D. A., Schmid, B., Russell, P. B., Livingston, J. M., Öström, E., Noone, K. J., Russell, L. M. and Putaud, J. P. 2000. In situ aerosol size distributions and clear column radiative closure during ACE-2. *Tellus*, 52B, No. 2, April 2000, pp. 498-525.
- Doherty, S.J., T.L. Anderson and R.J. Charlson, Measurement of the lidar ratio for atmospheric aerosols using a 180-degree backscatter nephelometer, *Appl. Opt.*, 38, 1823-1832, 1999.
- Dubovik, O., B. Holben, T. F. Eck, A. Smirnov, Y. J. Kaufman, M. D. King, D. Tanré, and I. Slutsker, Variability of absorption and optical properties of key aerosol types observed in worldwide locations, *J. Atmos. Sci.*, 59, 590-608, 2002.
- Eck, T. F., B. N. Holben, J. S. Reid, O. Dubovik, A. Smirnov, N. T. O'Neill, I. Slutsker, and S. Kinne, Wavelength dependence of the optical depth of biomass burning, urban, and desert dust aerosols, *J. Geophys. Res.*, 104, 31,333-31,349, 1999.
- Hansen, J., M. Sato, and R. Ruedy, Radiative forcing and climate response, *J. Geophys. Res.*, 102, 6831-6864, 1997.

- Harder J. W., J. W. Brault, P. V. Johnston, and G. H. Mount, Temperature dependent NO₂ cross sections at high spectral resolution, *J. Geophys. Res.*, *102*, 3861-3879, 1997.
- Hartley, W. S., Hobbs, P. V., Ross, J. L., Russell, P. B., and Livingston, J. M. Properties of aerosols aloft relevant to direct radiative forcing off the mid-Atlantic coast of the United States. *J. Geophys. Res.*, Vol. 105 , No. D8 , 9859-9886 (2000).
- Hegg D.A., J. Livingston, P.V. Hobbs, T. Novakov, and P. Russell, Chemical apportionment of aerosol column optical depth off the mid-Atlantic coast of the United States, *J. Geophys. Res.*, *102*, 25,293-25,303, 1997.
- Holben, B. N., T. Eck, I. Slutsker, D. Tanré, J. B. Buis, A. Setzer, E. Vermote, J. A. Reagan, Y. J. Kaufman, T. Nakajima, F. Lavenu, I. Jankowiak, and A. Smirnov, AERONET – A Federated Instrument Network and Data Archive for Aerosol Characterization. *Rem. Sens. Env.*, *66*, 1-16, 1998.
- Huebert B., T. Bates, P. B. Russell, K. Kawamura, Y. J. Kim, S. Guangyu. An overview of ACE-Asia, an Asian and Pacific regional aerosol characterization experiment. To be submitted to *J. Geophys. Res.*, 2002.
- Kasten, F., Visibility in the phase of pre-condensation, *Tellus*, *21*, 631-635, 1969.
- Kinne, S., T. P. Ackerman, M. Shiobara, A. Uchiyama, A. J. Heymsfield, L. Milosevich, J. Wendell, E. W. Eloranta, C. Purgold, and R. W. Bergstrom, Cirrus cloud radiative and microphysical properties from ground observations and in situ measurements during FIRE 1991 and their application to exhibit problems in cirrus solar radiative transfer modeling, *J. Atmos. Sci.*, *54*, 2320-2344, 1997.
- Livingston, J. M., P.B. Russell, J.S. Reid, J. Redemann, B. Schmid, D.A. Allen, O. Torres, R.C. Levy, L.A. Remer, B.N. Holben, A. Smirnov, O. Dubovik, E.J. Welton, J.R. Campbell, J. Wang, S.A. Christopher, Airborne sunphotometer measurements of aerosol optical depth and

- columnar water vapor during the Puerto Rico Dust Experiment, and comparison with land, aircraft, and satellite measurements, *J. Geophys. Res.*, accepted, 2002.
- Magi, B. I., P. V. Hobbs, B. Schmid, and J. Redemann, Vertical profiles of light scattering, light absorption and single scattering albedo during the dry, biomass burning season in southern Africa and comparisons of in situ and remote sensing measurements of aerosol optical depths, *J. Geophys. Res.*, in press, 2002.
- Masonis, S.J., K. Franke, A. Ansmann, D. Mueller, D. Althausen, J.A. Ogren, A. Jefferson, P.J. Sheridan, An intercomparison of aerosol light extinction and 180° backscatter as derived using in situ instruments and Raman lidar during the INDOEX field campaign, *J. Geophys. Res.*, 10.1029/2000JD000035, 04 September 2002.
- Matsumoto, T., P. B. Russell, C. Mina, W. Van Ark and V. Banta, 1987: Airborne Tracking Sunphotometer. *J. Atmos. Ocean. Tech.*, Vol. 4, 336-339.
- Ramanathan, V., P.J. Crutzen, J.T. Kiehl, and D. Rosenfeld, Aerosol, Climate and the Hydrological Cycle, *Science*, 294, 2119-2124, 2001.
- Redemann, J., Schmid, B., Livingston, J. M., Russell, P. B., Eilers, J. A., Hobbs, P. V., Kahn, R. , Smith, W. L., Holben, B. N., Rutledge, C. K., Pitts, M. C., Mishchenko, M. I., Chowdhary, J. , Martins, J. V., Plana-Fattori, A., Charlock, T. P., Combining Suborbital Measurements of Aerosol Optical Depth and Columnar Water Vapor for Satellite Sensor Validations in the CLAMS (Chesapeake Lighthouse and Aircraft Measurements for Satellites) Experiment, 2001, *EOS Transactions*, Vol.83, no. 19, pp.S22-23, 2002.
- Rothman L.S., K. Chance, J. Schroeder, and A. Goldman. New Edition of HITRAN Database. 11th ARM Science Team Meeting Proceedings, Atlanta, Georgia, March 19-23, 2001.
- Russell, P. B., P. V. Hobbs, and L. L. Stowe, Aerosol properties and radiative effects in the United States Mid-Atlantic haze plume: An overview of the Tropospheric Aerosol Radiative Forcing Observational Experiment (TARFOX), *J. Geophys. Res.*, 104, 2213-2222, 1999a.

- Russell, P. B., J. M. Livingston, P. Hignett, S. Kinne, J. Wong, and P. V. Hobbs, Aerosol-induced radiative flux changes off the United States Mid-Atlantic coast: Comparison of values calculated from sunphotometer and in situ data with those measured by airborne pyranometer, *J. Geophys. Res.*, *104*, 2,289-2,307, 1999b.
- Russell, P. B., J. M. Livingston, E. G. Dutton, R. F. Pueschel, J. A. Reagan, T. E. Defoor, M. A. Box, D. Allen, P. Pilewskie, B. M. Herman, S. A. Kinne, and D. J. Hofmann, Pinatubo and pre-Pinatubo optical-depth spectra: Mauna Loa measurements, comparisons, inferred particle size distributions, radiative effects, and relationship to lidar data. *J. Geophys. Res.*, *98*, 22,969-22,985, 1993a.
- Russell, P.B., J. M. Livingston, R. F. Pueschel, J. A. Reagan, E.V. Browell, G. C. Toon, P.A. Newman, M.R. Schoeberl, L.R. Lait, L. Pfister, Q. Gao, and B. M. Herman, "Post-Pinatubo Optical Depth Spectra vs. Latitude and Vortex Structure: Airborne Tracking Sunphotometer Measurements in AASE II," *Geophys. Res. Lett.*, *20*, 2571-2574, 1993b.
- Schmid, B., and C. Wehrli, Comparison of sun photometer calibration by Langley technique and standard lamp, *Appl. Opt.*, *34*, 4500-4512, 1995.
- Schmid, B., K. J. Thome, P. Demoulin, R. Peter, C. Mätzler, and J. Sekler, Comparison of modeled and empirical approaches for retrieving columnar water vapor from solar transmittance measurements in the 0.94 micron region, *J. Geophys. Res.*, *101*, 9345-9358, 1996.
- Schmid, B., D.A. Hegg, J. Wang, D. Bates, J. Redemann, P.B. Russell, J.M. Livingston, H.H. Jonsson, E.J. Welton, J.H. Seinfeld, R.C. Flagan, D.S. Covert, O. Dubovik, and A. Jefferson, Column closure studies of lower tropospheric aerosol during ACE-Asia using airborne sunphotometer, airborne in-situ and ship-based lidar measurements, this issue, 2003.
- Schmid B., J. Redemann, P. B. Russell, P. V. Hobbs, D. L. Hlavka, M. J. McGill, B. N. Holben, E. J. Welton, J. Campbell, O. Torres, R. A. Kahn, D. J. Diner, M. C. Helmlinger, D. A. Chu,

- C. Robles Gonzalez, and G. de Leeuw, Coordinated airborne, spaceborne, and ground-based measurements of massive, thick aerosol layers during the dry season in Southern Africa, *J. Geophys. Res.*, in press, 2002.
- Schmid, B., J. M. Livingston, P. B. Russell, P. A. Durkee, H. H. Jonsson, D. R. Collins, R. C. Flagan, J. H. Seinfeld, S. Gassó, D. A. Hegg, E. Öström, K. J. Noone, E. J. Welton, K. Voss, H. R. Gordon, P. Formenti, and M. O. Andreae, Clear sky closure studies of lower tropospheric aerosol and water vapor during ACE-2 using airborne sunphotometer, airborne in-situ, space-borne, and ground-based measurements, *Tellus*, 52B, 568-593, 2000.
- Sprent and Dolby, The Geometric Mean Functional Relationship, *Biometrics*, 36, 547-550, 1980.
- Wang J., R. C. Flagan, J. H. Seinfeld, H. H. Jonsson, D. R. Collins, P. B. Russell, B. Schmid, J. Redemann, J. M. Livingston, S. Gao, D. A. Hegg, E. J. Welton, and D. Bates. Clear-column radiative closure during ACE-Asia: Comparison of multiwavelength extinction derived from particle size and composition with results from sunphotometry, *J. Geophys. Res.*, in press, 2002.

7. Tables

Table 1. Comparison of 550nm aerosol extinction as derived from the AATS-6 and in situ method (cf. Figure 6), stratified by ambient relative humidity, RH. Model II line-fit parameters for least-square bisectors are given in the form $y=mx+b$. The least-square bisector method uses the bisector of the minor angle between the two model I linear-least square regression fits, x-on-y and y-on-x. σ_m and σ_b are the standard deviations of the slope and intercept respectively, calculated as the symmetrical limits for a model I regression, using formulations from *Bevington and Robinson* (1992, pp. 108-109).

RH range	m	b	r^2	σ_m	σ_b	# of data points in RH range
all RH	1.06	-0.005	0.792	0.008	0.001	3555
0-20%	0.76	0.001	0.467	0.014	0.001	1965
20-40%	1.02	0.001	0.811	0.018	0.001	632
40-60%	1.28	-0.011	0.871	0.023	0.002	416
60-80%	1.04	-0.009	0.848	0.020	0.002	453
80-100%	1.27	-0.014	0.766	0.069	0.009	86

Table 2. Comparison of 550nm aerosol extinction as derived from the AATS-6 and in situ method (cf. Figure 7), stratified by fine mode scattering fraction, FFscat (defined here as the fraction of dry light scattering due to aerosols smaller than 1 μ m in diameter). Model II line-fit parameters for least-square bisectors are given in the form $y=mx+b$. The least-square bisector method uses the bisector of the minor angle between the two model I linear-least square regression fits, x-on-y and y-on-x. σ_m and σ_b are the standard deviations of the slope and intercept respectively, calculated as the symmetrical limits for a model I regression, using formulations from *Bevington and Robinson* (1992, pp. 108-109).

FFscat range	m	b	r^2	σ_m	σ_b	# of data points in FFscat range
all	1.06	-0.006	0.786	0.009	0.001	3384
<30%	1.13	-0.005	0.715	0.018	0.001	1243
30-60%	1.12	-0.010	0.779	0.016	0.001	1198
60-100%	1.01	-0.004	0.807	0.015	0.001	943

Table 3. Comparison of Ångström exponents derived from AATS-6 extinction spectra and in situ measured dry scattering between 450 and 700 nm (cf. Figure 9), stratified by ambient relative humidity, RH. Model II line-fit parameters for least-square bisectors are given in the form $y=mx+b$. The least-square bisector method uses the bisector of the minor angle between the two model I linear-least square regression fits, x-on-y and y-on-x. σ_m and σ_b are the standard deviations of the slope and intercept respectively, calculated as the symmetrical limits for a model I regression, using formulations from *Bevington and Robinson* (1992, pp. 108-109).

RH range	m	b	r^2	σ_m	σ_b	# of data points in RH range
all	1.00	0.091	0.620	0.013	0.013	2490
<40%	0.95	0.088	0.610	0.015	0.015	1684
>40%	1.05	0.120	0.517	0.028	0.032	806

8. Figure captions

Figure 1. Location of 28 profiles used in the closure study presented here.

Figure 2. Vertical distribution of AATS-6 derived aerosol optical depth, $\tau_p(\lambda)$, at four wavelengths (380.1, 450.9, 525.7, and 1021.3nm) for the 28 profiles indicated in Figure 1.

Figure 3. Vertical distribution of aerosol extinction, $\sigma_{ep}(\lambda)$, at the same wavelengths as shown in Figure 2. Extinction profiles were obtained by binning the $\tau_p(\lambda)$ measurements into 50m altitude bins, fitting smoothed cubic spline functions to the binned $\tau_p(\lambda)$, and subsequent differentiation of the smoothed spline fits with respect to altitude.

Figure 4. Vertical distribution of the AATS-6 derived extinction Ångström exponent, obtained by fitting Ångström laws to the extinction spectra at each altitude (blue dots). Ångström exponents are shown at altitudes where $\sigma_{ep}(550\text{nm})$ exceeded 0.01km^{-1} . Shown for comparison are in situ derived scattering Ångström exponents, calculated by fitting Ångström laws to the spectra of TSI nephelometer derived scattering between 450 and 700nm (green dots).

Figure 5. Vertical distribution of aerosol extinction at 550nm calculated from AATS-6 (blue lines and dots) and a combination of humidified nephelometer derived scattering and PSAP derived aerosol absorption (green lines and dots).

Figure 6. Comparison of AATS-6 derived and in situ derived aerosol extinction at 550nm. Stratification of data into 20% RH intervals is indicated. The fit lines represent least square bisector method fits (see text). Values for the fit parameters and their uncertainties can be found in Table 1.

Figure 7. Comparison of AATS-6 derived and in situ derived aerosol extinction at 550nm. Stratification of data by FFscat intervals is indicated. The fit lines represent least square bisector method fits (see text). Values for the fit parameters and their uncertainties can be found in Table 2.

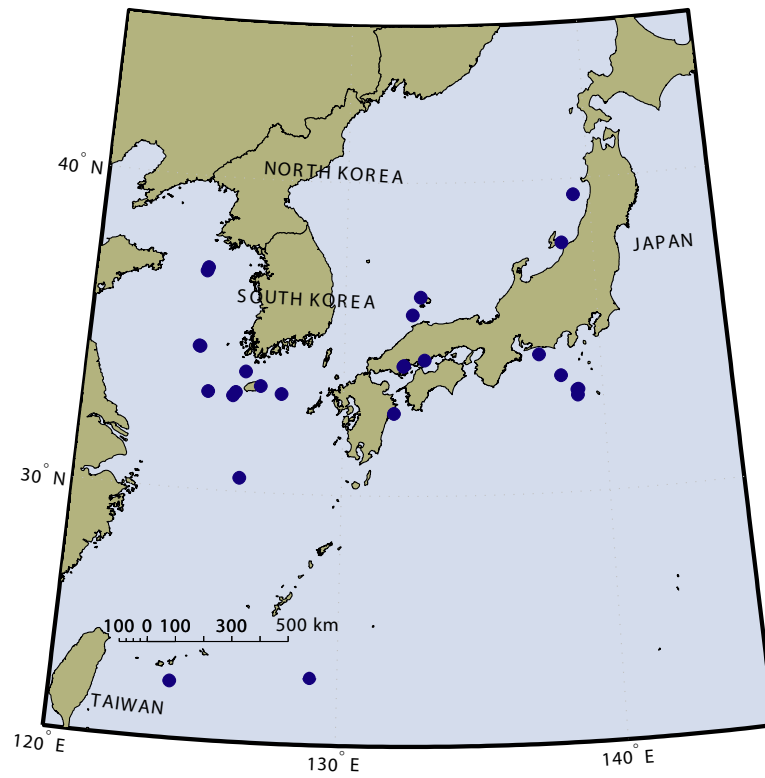
Figure 8. Comparison of layer aerosol optical depth at 550nm. In situ derived layer optical depths were calculated as the vertical integral of extinction profiles shown in Figure 5. AATS-6 derived values are calculated as the differences between $\tau_p(550)$ at the bottom and top of the same profiles. Dark blue AATS-6 uncertainties represent uncertainties due to potential horizontal gradients, while light blue error bars are due to instrumental uncertainties (see text, Eqn. 7+9).

Figure 9. Comparison of Ångström exponents presented in Figure 4. Stratification by ambient relative humidity is indicated. The fit lines represent least square bisector method fits (see text). Values for the fit parameters and their uncertainties can be found in Table 3.

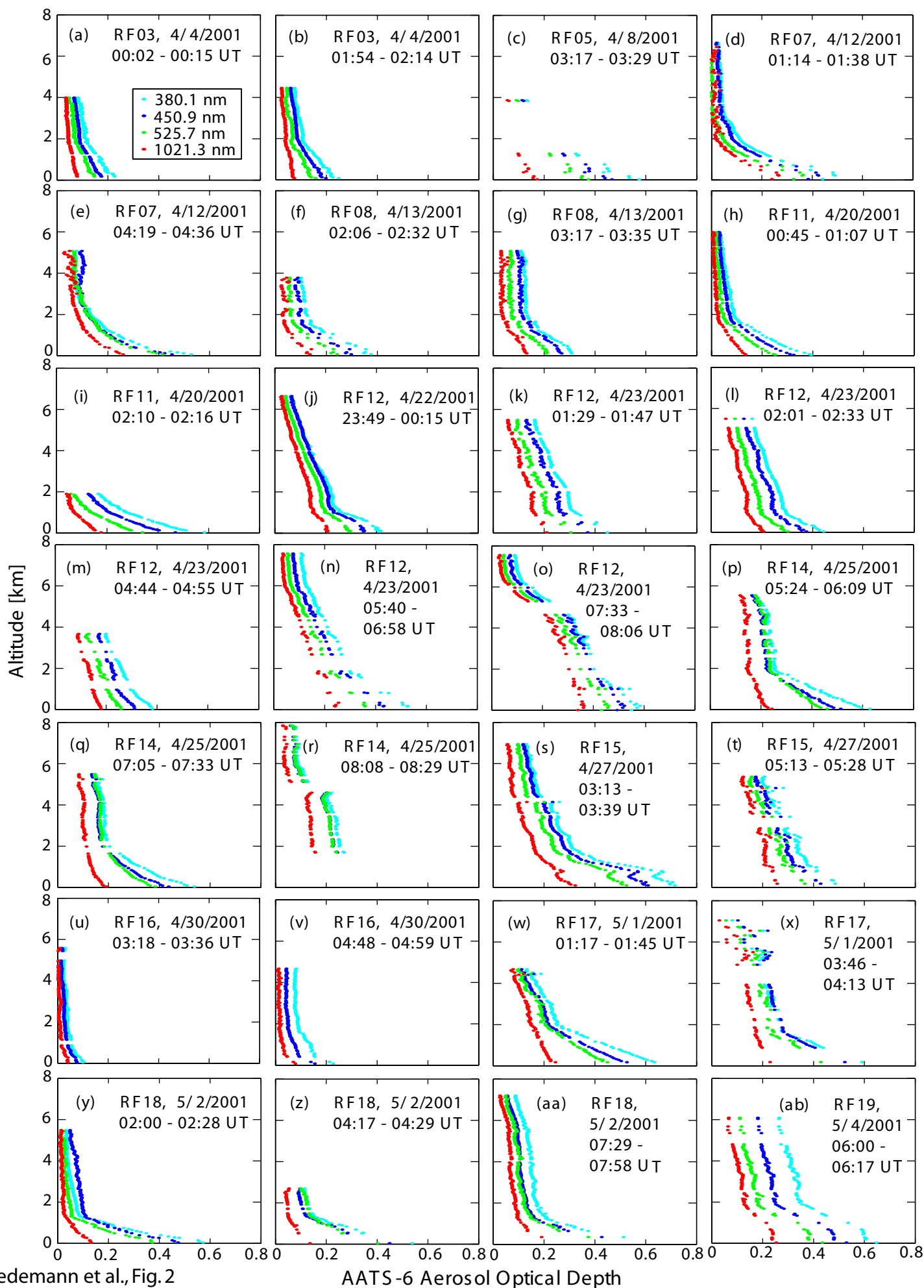
Figure 10. Like Figure 2, but for the vertical distribution of AATS-6 derived water vapor density (blue). For comparison, the in situ humidity measurements taken by the NCAR RAF reference sensors are shown (green).

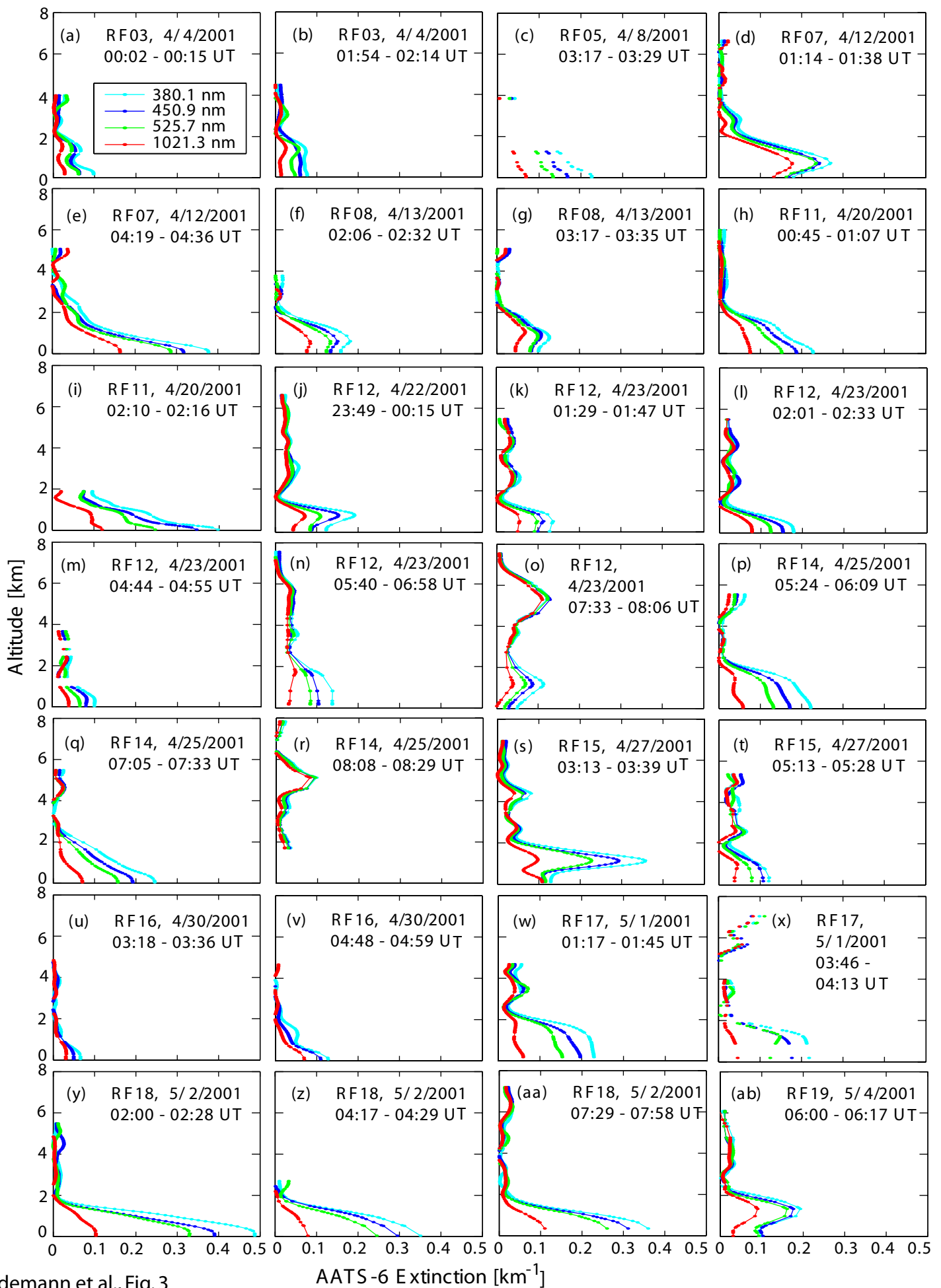
Figure 11. Like Figure 8, but for layer water vapor. The in situ derived layer water vapor values are obtained by integrating the vertical profiles water vapor density (shown in Figure 10). The fit lines represent model I least square regressions of X-on-Y (see text), because the in situ measurements are considered the standard by which AATS-6 measurements need to be evaluated. Values for the fit parameters are given as text inserts.

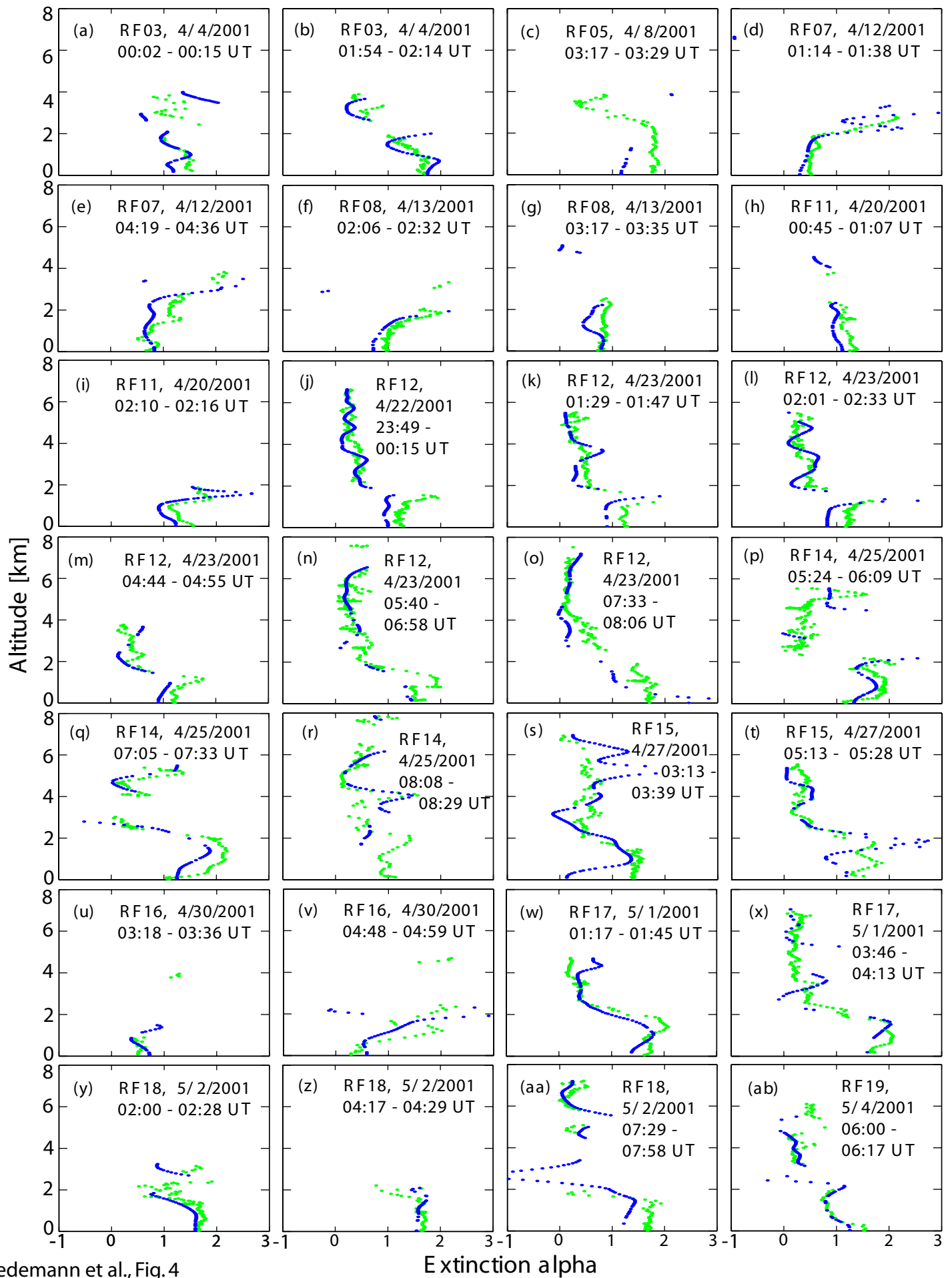
Figure 12. Comparison of water vapor density from AATS-6 and in situ humidity measurements. The fit lines represent model I least square regressions of X-on-Y (see text), because the in situ measurements are considered the standard by which AATS-6 measurements need to be evaluated. Values for the fit parameters are given as text inserts.

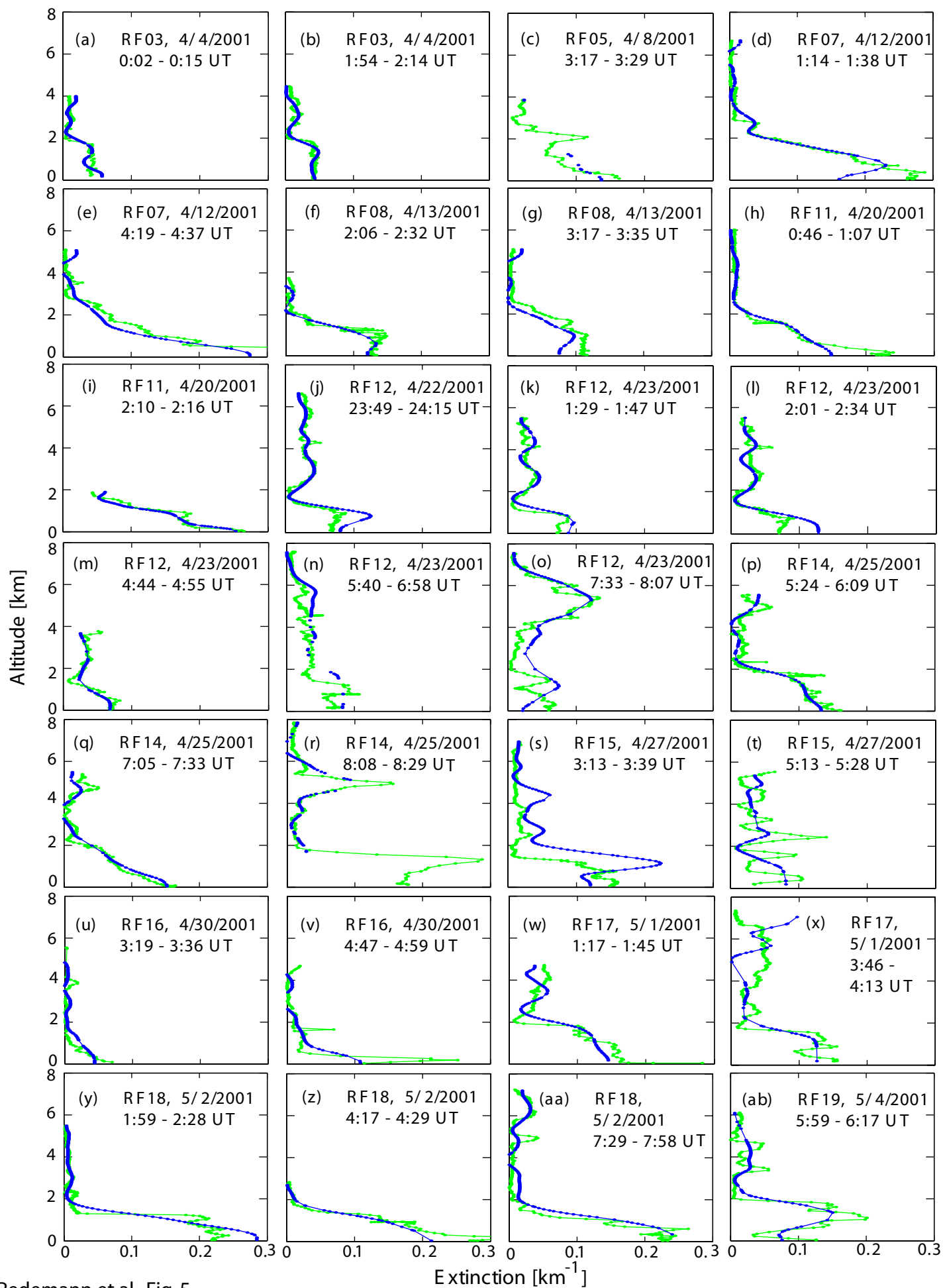


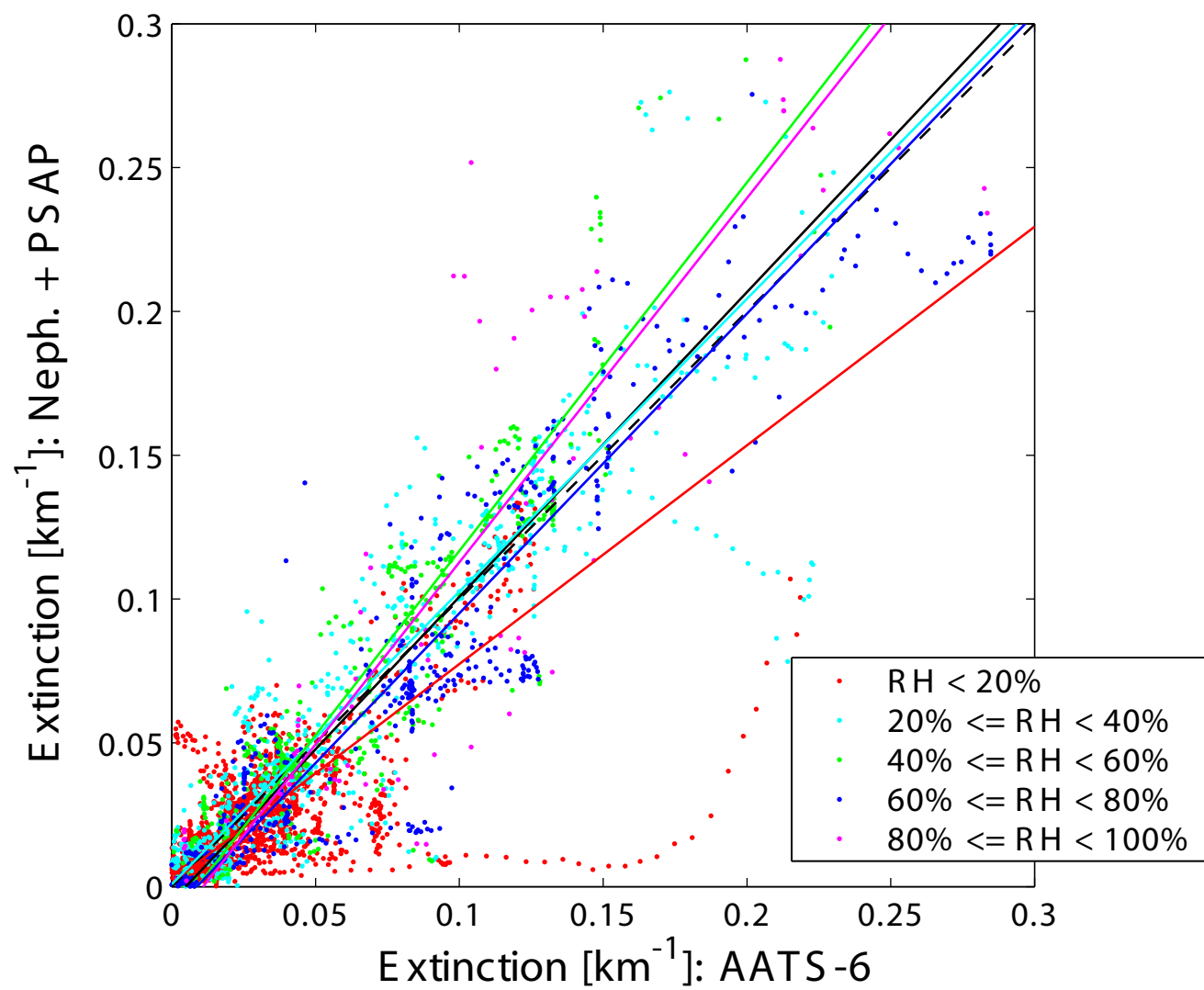
Redemann et al., Fig. 1



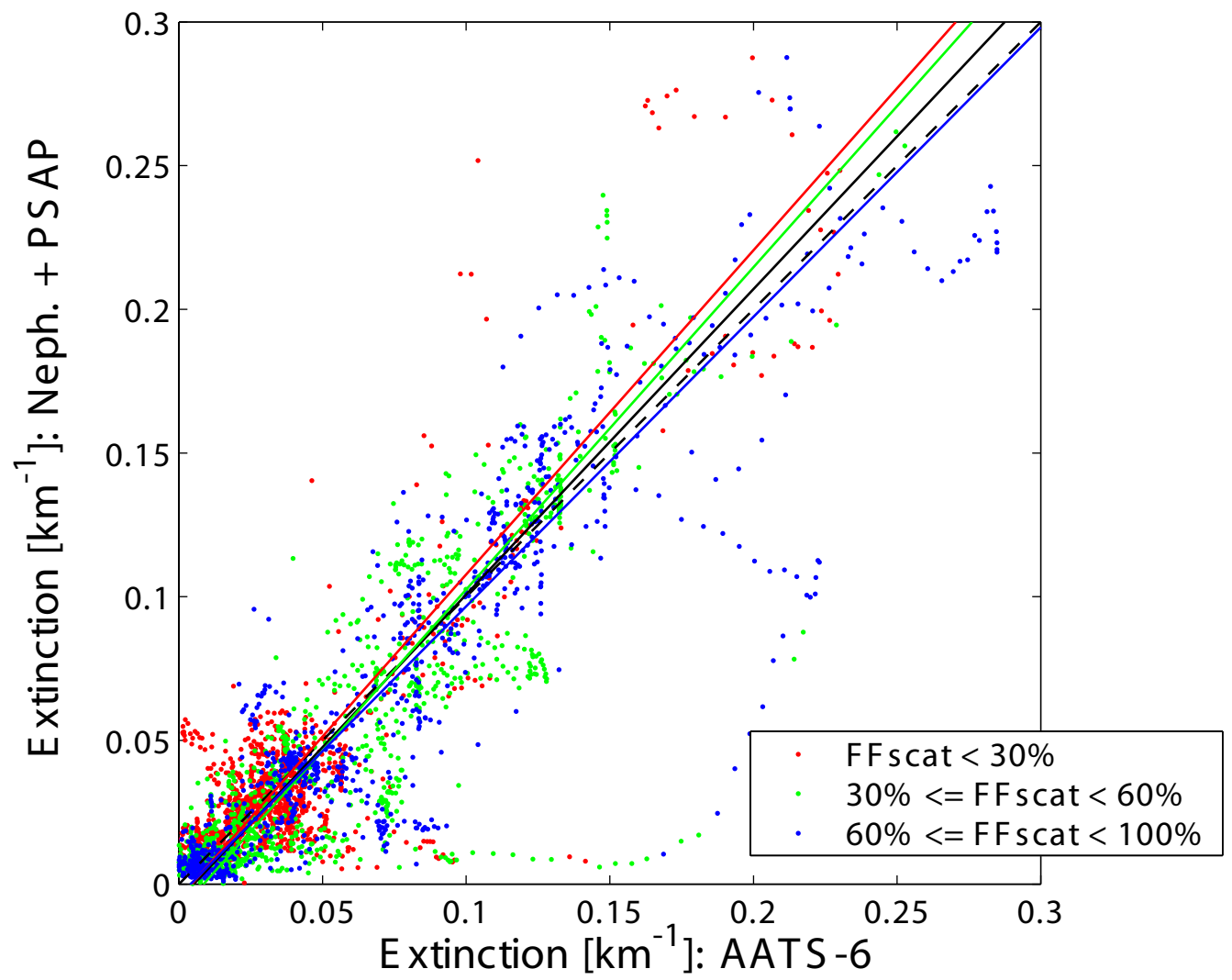




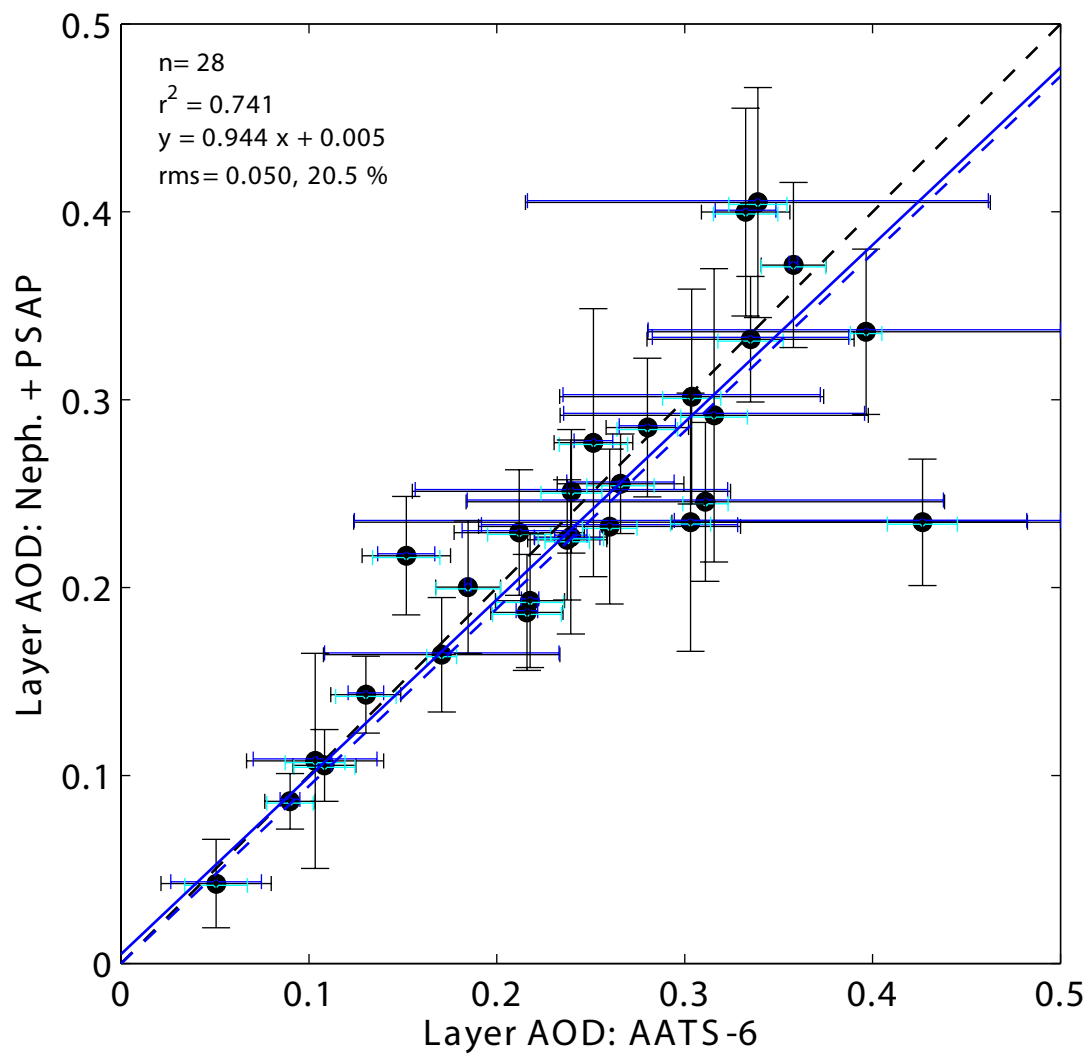




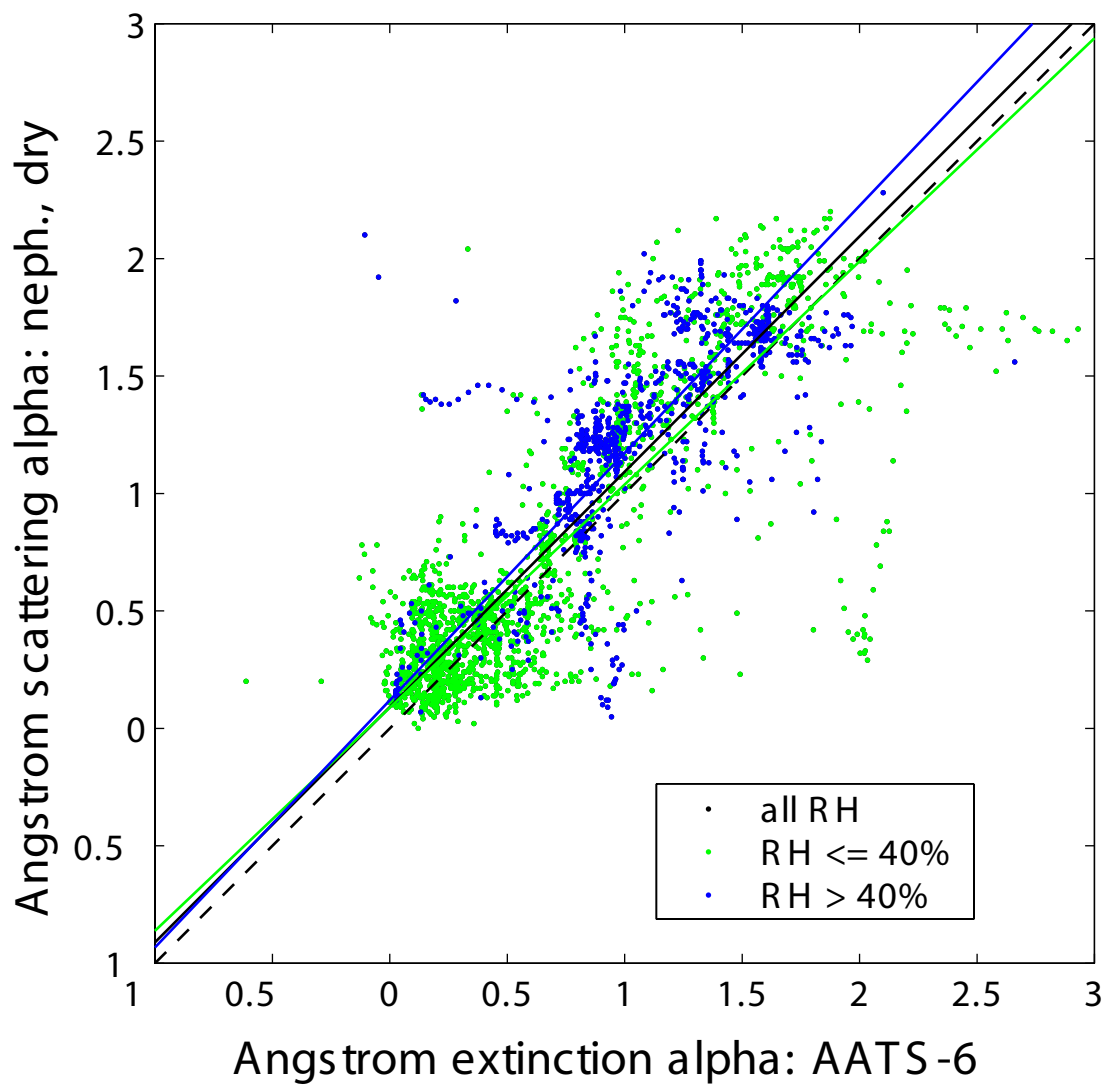
Redemann et al., Fig. 6



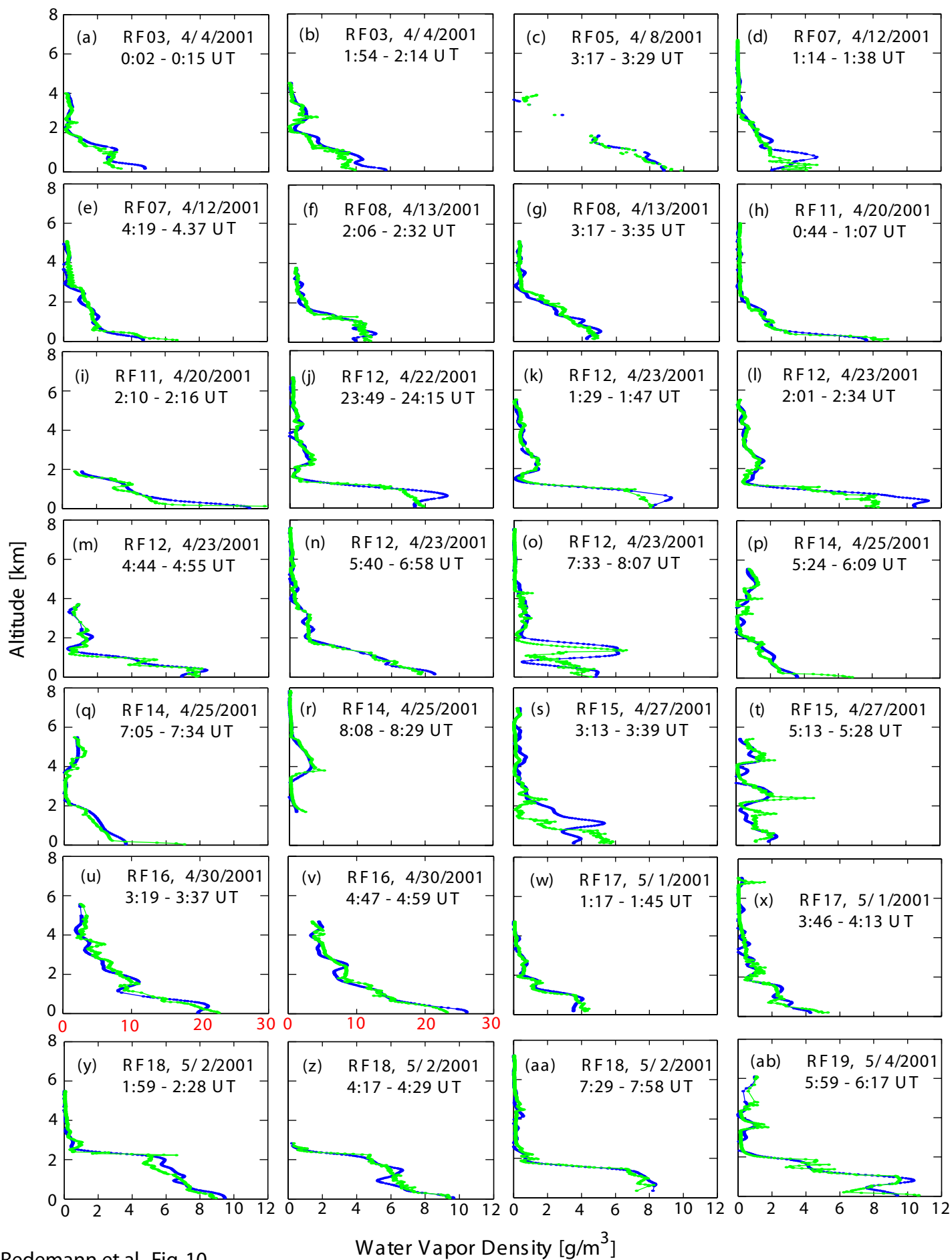
Redemann et al., Fig. 7



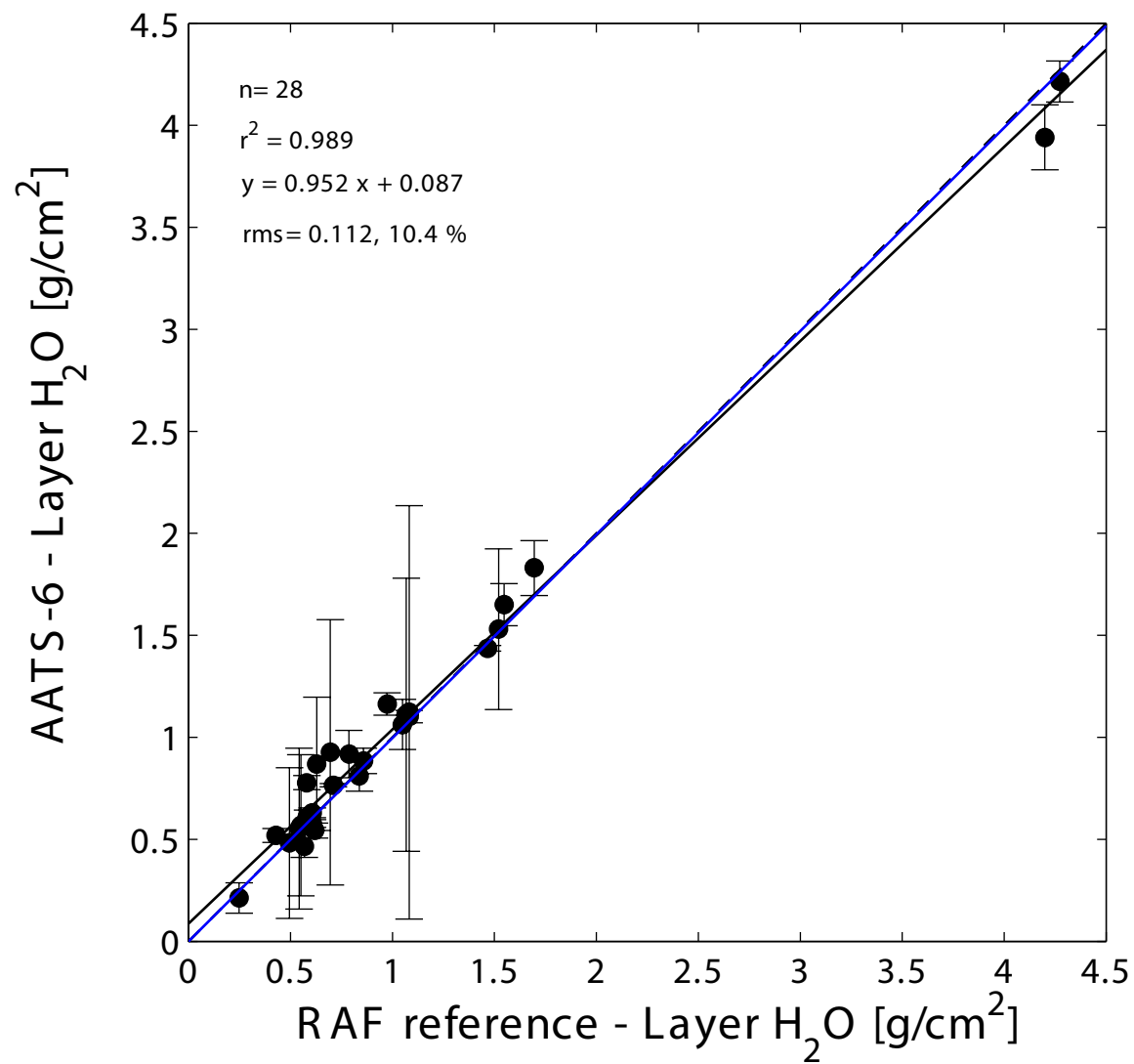
Redemann et al., Fig. 8



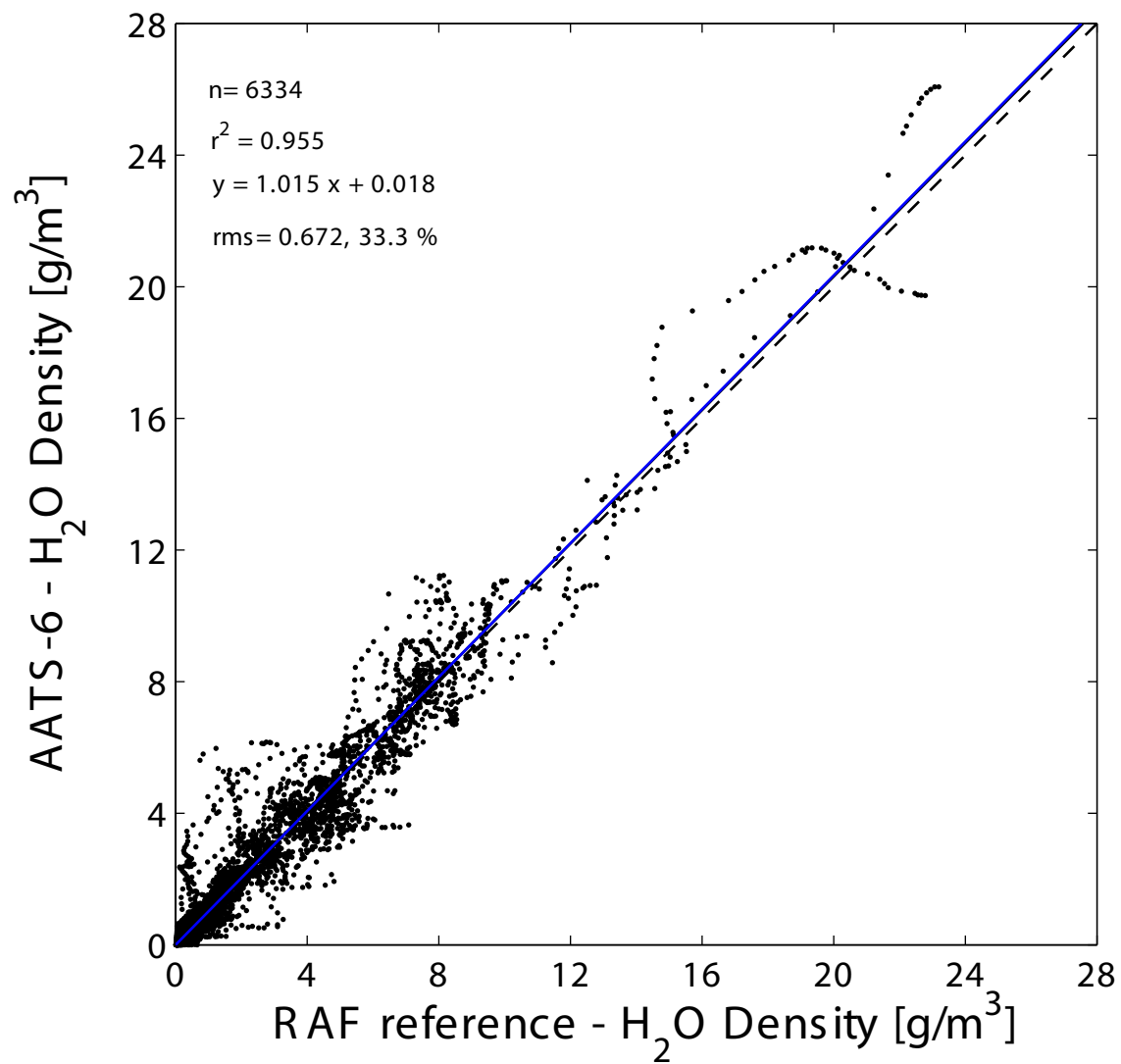
Redemann et al. Fig. 9



Redemann et al., Fig. 10



Redemann et al., Fig. 11



Redemann et al., Fig. 12